Molecular Therapy
Original Article

Risk-Associated Long Noncoding RNA FOXD3-AS1 Inhibits Neuroblastoma Progression by Repressing PARP1-Mediated Activation of CTCF

Xiang Zhao,[1,4] Dan Li,[1,4] Dandan Huang,[2,4] Huajie Song,[1,4] Hong Mei,[1] Erhu Fang,[1] Xiaojing Wang,[1] Feng Yang,[1] Liduan Zheng,[2,3] Kai Huang,[2] and Qiangsong Tong[1,2]

[1]Department of Pediatric Surgery, Union Hospital, Tongji Medical College, Huazhong University of Science and Technology, 1277 Jiefang Avenue, Wuhan 430022, Hubei Province, China; [2]Clinical Center of Human Genomic Research, Union Hospital, Tongji Medical College, Huazhong University of Science and Technology, 1277 Jiefang Avenue, Wuhan 430022, Hubei Province, China; [3]Department of Pathology, Union Hospital, Tongji Medical College, Huazhong University of Science and Technology, 1277 Jiefang Avenue, Wuhan 430022, Hubei Province, China

Neuroblastoma (NB) is the most common extracranial tumor in childhood. Recent studies have implicated the emerging roles of long noncoding RNAs (lncRNAs) in tumorigenesis and aggressiveness. However, the functions and targets of risk-associated lncRNAs in NB progression still remain to be determined. Herein, through mining of public microarray datasets, we identify lncRNA forkhead box D3 antisense RNA 1 (FOXD3-AS1) as an independent prognostic marker for favorable outcome of NB patients. FOXD3-AS1 is downregulated in NB tissues and cell lines, and ectopic expression of *FOXD3-AS1* induces neuronal differentiation and decreases the aggressiveness of NB cells *in vitro* and *in vivo*. Mechanistically, as a nuclear lncRNA, FOXD3-AS1 interacts with poly(ADP-ribose) polymerase 1 (PARP1) to inhibit the poly(ADP-ribosyl)ation and activation of CCCTC-binding factor (CTCF), resulting in derepressed expression of downstream tumor-suppressive genes. Rescue experiments indicate that FOXD3-AS1 harbors tumor-suppressive properties by inhibiting the oncogenic roles of PARP1 or CTCF and plays crucial roles in all-*trans*-retinoic-acid-mediated therapeutic effects on NB. Administration of *FOXD3-AS1* construct or siRNAs against *PARP1* or *CTCF* reduces the tumor growth and prolongs the survival of nude mice. These findings suggest that as a risk-associated lncRNA, FOXD3-AS1 inhibits the progression of NB through repressing PARP1-mediated CTCF activation.

INTRODUCTION

Neuroblastoma (NB) is the most common extracranial malignant solid tumor in childhood and accounts for 15% of all cancer-related deaths in the pediatric population. NB is characterized by remarkable heterogeneity in biological behaviors, ranging from spontaneous regression to rapid progression.[1] For high-risk NB patients, many therapeutic modalities fail to improve the clinical outcome.[2] Thus, the mechanisms underlying the progression of NB still remain to be determined to improve the therapeutic efficiency.

Recent evidence has shown the emerging roles of long noncoding RNA (lncRNA) in the pathogenesis of NB. For example, neuroblastoma differentiation marker 29 (NDM29) is underexpressed in NB, and ectopic expression of *NDM29* exhibits tumor-suppressive properties.[3] Loss of neuroblastoma-associated transcript-1 (*NBAT1*) contributes to NB progression via increasing proliferation and reducing differentiation of neuronal precursors.[4] lncRNA transcribed upstream the transcription start site of *MYCN* (LncUSMycN) binds to non-POU-domain-containing octamer-binding protein to facilitate MYCN expression and proliferation of NB cells.[5] In addition, paired box 6 upstream antisense RNA (Paupar) regulates the expression of genes on multiple chromosomes, and knockdown of *Paupar* disrupts cell-cycle progression and induces neuronal differentiation of NB cells.[6] Our previous studies show that lncRNA MYCN opposite strand (MYCNOS) cooperates with CCCTC-binding factor (CTCF) to promote NB progression by facilitating MYCN expression.[7] However, the identification of lncRNAs associated with death, progression, and advanced stages of NB has not been described.

In the current study, mining of public microarray datasets was performed to explore lncRNA-based biomarkers for risk assessment and therapeutics of NB. We identified a 963-bp lncRNA forkhead box D3 antisense RNA 1 (FOXD3-AS1) as an independent prognostic

Received 21 August 2017; accepted 18 December 2017;
https://doi.org/10.1016/j.ymthe.2017.12.017.

[4]These authors contributed equally to this work.

Correspondence: Qiangsong Tong, Department of Pediatric Surgery, Union Hospital, Tongji Medical College, Huazhong University of Science and Technology, Wuhan 430022, Hubei Province, China.
E-mail: qs_tong@hotmail.com
Correspondence: Kai Huang, Clinical Center of Human Genomic Research, Union Hospital, Tongji Medical College, Huazhong University of Science and Technology, Wuhan 430022, Hubei Province, China.
E-mail: huangkai1@hust.edu.cn
Correspondence: Liduan Zheng, Department of Pathology, Union Hospital, Tongji Medical College, Huazhong University of Science and Technology, Wuhan 430022, Hubei Province, China.
E-mail: ld_zheng@hotmail.com

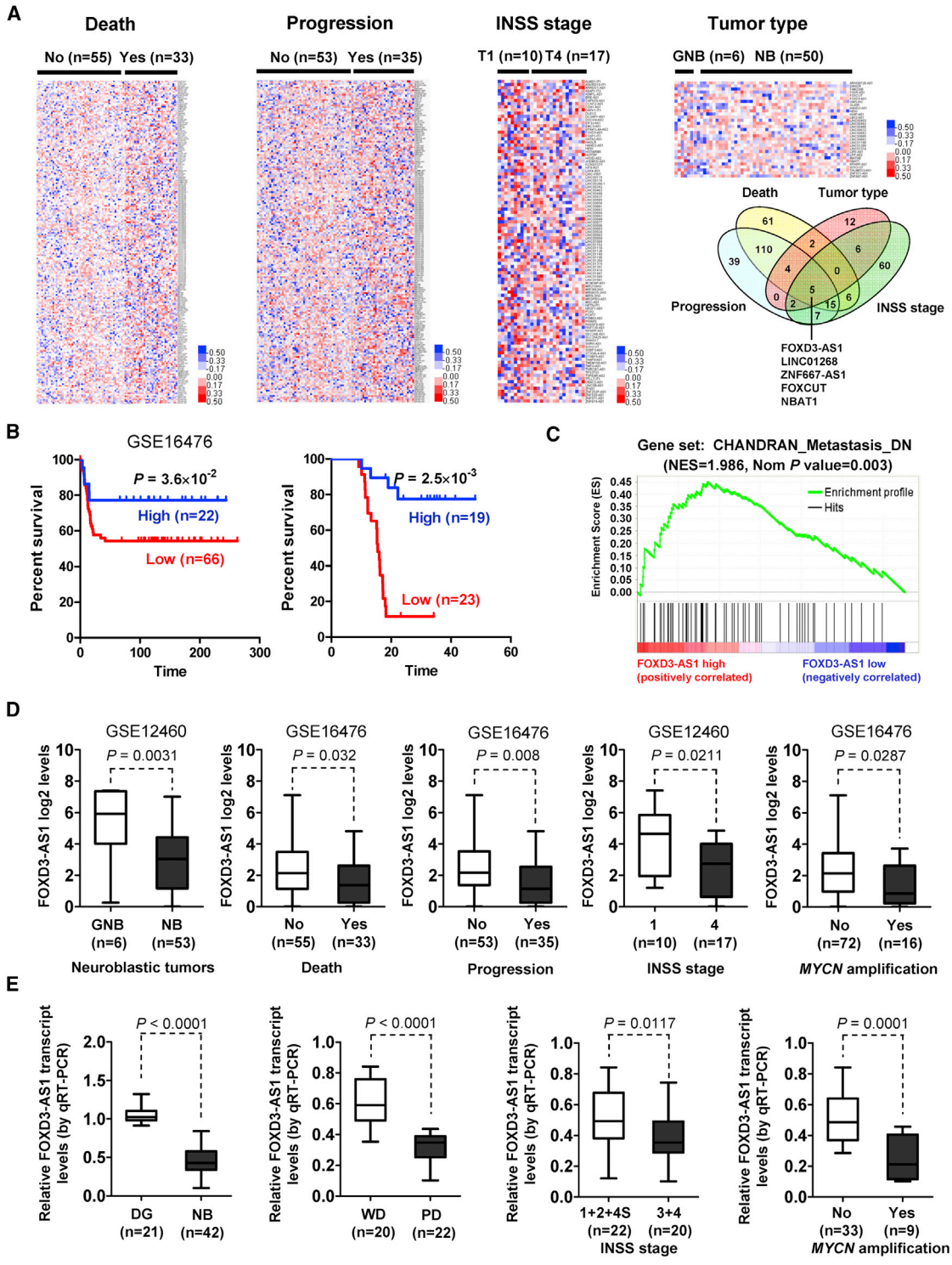

Figure 1. Identification of FOXD3-AS1 As an Independent Prognostic Marker for NB Progression

(A) Cluster analysis and heatmap (left, middle, and right top panels) of microarray datasets (GEO: GSE16476 and GSE12460) in 88 NB and 64 neuroblastic tumors derived from the GEO depicting the differentially expressed lncRNAs ($p < 0.05$, FDR < 0.05) in tumors with various status of death, progression, INSS stage, and tumor type. Venn diagram (right bottom panel) indicating the identification of lncRNAs consistently associated with death, progression, advanced INSS stages, and aggressive neuroblastic tumors. (B) Kaplan-Meier curves indicating survival of 88 (GEO: GSE16476) and 42 NB patients with high or low FOXD3-AS1 expression (cutoff values = 8.3 and 0.455).

(legend continued on next page)

marker for favorable outcome of NB patients. We demonstrate that FOXD3-AS1 is downregulated in NB tissues and cell lines. Ectopic expression of *FOXD3-AS1* induces neuronal differentiation and inhibits the growth, invasion, and metastasis of NB cells *in vitro* and *in vivo*. Mechanistically, FOXD3-AS1 binds to poly(ADP-ribose) polymerase 1 (PARP1) to inhibit the poly(ADP-ribosyl)ation (PARylation) and activation of epigenetic regulator CTCF, resulting in derepressed expression of downstream tumor-suppressive genes. Administration of *FOXD3-AS1* construct and small interfering RNAs (siRNAs) against *PARP1* or *CTCF* reduces tumor growth and prolongs the survival of nude mice bearing xenografts, indicating the crucial roles of FOXD3-AS1 in the progression of NB.

RESULTS

Identification of lncRNA FOXD3-AS1 As an Independent Prognostic Marker for NB Progression

To investigate the lncRNAs crucial for NB progression, mining of public microarray datasets of 88 NB cases (GEO: GSE16476) and 64 neuroblastic tumors (GEO: GSE12460) was performed. We found 203, 182, 101, and 31 differentially expressed lncRNAs ($p < 0.05$, false discovery rate [FDR] < 0.05) associated with the status of death, clinical progression, International Neuroblastoma Staging System (INSS) stage, or neuroblastic tumor type, respectively (Figure 1A). Comprehensive analysis of these lncRNAs ($p = 0.002$) identified 5 lncRNAs that were consistently associated with death, progression, advanced INSS stages, and aggressive neuroblastic tumors (Figure 1A), including FOXD3-AS1, LINC01268, ZNF667 antisense RNA 1 (ZNF667-AS1), FOXC1 upstream transcript (FOXCUT), and NBAT1.[4] Among them, FOXD3-AS1, LINC01268, and NBAT1 were associated with a favorable outcome in NB patients, while ZNF667-AS1 and FOXCUT were correlated with a poor prognosis (Table S1). A log-rank test and multivariate Cox regression analyses of 88 NB cases (GEO: GSE16476) revealed FOXD3-AS1 as the top independent prognostic factor (hazard ratio [HR] = 0.472; 95% confidence interval, 0.313 to 1.446; $p = 0.004$, Figure 1A; Table S1). Kaplan-Meier curves of 88 (GEO: GSE16476) and 42 NB cases showed highly significant difference in patients' survival ($p = 3.6 \times 10^{-2}$ and $p = 2.5 \times 10^{-3}$) between high and low FOXD3-AS1 expression groups (Figure 1B). Gene set enrichment analysis on all genes correlated to FOXD3-AS1 in 88 NB cases (GEO: GSE16476) yielded a significant association with the cancer metastasis gene signature (normalized enrichment score [NES] = 1.986, normalized $p = 0.003$; Figure 1C). Mining of public datasets (GEO: GSE16476 and GSE12460) revealed that FOXD3-AS1 levels were inversely associated with aggressiveness of neuroblastic tumors ($p = 0.0031$) and were lower in NB cases with death ($p = 0.032$), progression ($p = 0.008$), advanced INSS stages ($p = 0.0211$), or *MYCN* amplification ($p = 0.0287$; Figure 1D; Tables S2 and S3). In our cohort of 42 primary NB tumors, *FOXD3-AS1* was underexpressed ($p < 0.0001$) compared with normal dorsal ganglia (Figure 1E; Table S4). Lower *FOXD3-AS1* transcript levels were observed in NB cases with poor differentiation ($p < 0.0001$), advanced INSS stages ($p = 0.0117$), or *MYCN* amplification ($p = 0.0001$) (Figure 1E). These data indicated that lncRNA FOXD3-AS1 was an independent prognostic marker for NB progression.

Ectopic Expression of *FOXD3-AS1* Leads to Suppression of NB Progression

lncRNA *FOXD3-AS1* is consisted of four exons and is located at chromosome 1p31.3 upstream of the *FOXD3* promoter. Northern blot and 5′ and 3′ rapid amplification of cDNA ends (RACE) analyses confirmed the existence of a 963-bp polyadenylated *FOXD3-AS1* transcript in SH-SY5Y cells (Figures 2A and S1A). High FOXD3-AS1 levels were noted in the brain, heart, lung, spleen, and stomach tissues of human embryos (at day 50 of gestation; Figure S1B). Analysis using Coding Potential Assessment Tool (CPAT)[8] revealed a low value for *FOXD3-AS1* (coding probability = 0.0129). Ribosome profiling data[9] indicated low protein-coding potential of *FOXD3-AS1* (Figure S1C). Analysis of The Cancer Genome Atlas (TCGA) datasets indicated the upregulation of FOXD3-AS1 in esophageal cancer, endometrial cancer, renal cancer, or prostate cancer and downregulation in colon cancer and NB (Figure S1D). Mining of the public database revealed no copy-number alterations in the *FOXD3-AS1* gene locus (chromosome 1 [chr1]: 63786555–63788129) within NB tissues (Figure S1E). Lower FOXD3-AS1 expression was observed in cultured NB cell lines, especially in *MYCN*-amplified NB-1643, SK-N-BE(2), NB-1691, IMR32, and BE(2)-C (Figure 2B). Although mining of the public dataset (GEO: GSE28019) also revealed lower FOXD3-AS1 levels in *MYCN*-amplified NB cell lines than in those without *MYCN* amplification, the difference was not statistical significant ($p = 0.205$; Figure S1F).

The functional impact of *FOXD3-AS1* overexpression was then investigated in NB cells with low expression levels. Stable transfection of *FOXD3-AS1* into IMR32 and BE(2)-C cells reduced the number of viable cells compared to those transfected with empty vector (mock; Figures 2C and 2D). Annexin V/fluorescein isothiocyanate (FITC) and propidium iodide (PI) staining flow cytometry assay indicated that ectopic expression of *FOXD3-AS1* slightly induced the apoptosis of NB cells (Figure S2A). In addition, stable overexpression of *FOXD3-AS1* decreased the invasiveness of IMR32 and BE(2)-C cells (Figure 2E). Moreover, increased expression of neuronal differentiation markers (growth associated protein 43 [GAP43] and neurofilament heavy polypeptide [NF-200]) and facilitated neurite outgrowth were observed in cultured BE(2)-C cells following

(C) Gene set enrichment analysis of FOXD3-AS1-correlated genes in 88 NB tissues derived from a publically available dataset (GEO: GSE16476). NES, normalized enrichment score; Nom, normalized. (D) Mining of microarray datasets (GEO: GSE16476 and GSE12460) revealing the FOXD3-AS1 levels in tumor tissues with different tumor type or various status of death, progression, INSS stage, or *MYCN* amplification. (E) Real-time qRT-PCR assay revealing the differential expression of *FOXD3-AS1* transcript (normalized to GAPDH) in normal dorsal ganglia (DG; n = 21), NB tissues (n = 42) with poor (PD) or well differentiation (WD), and different INSS stages or *MYCN*-amplification status. Fisher's exact test for overlapping analysis is shown in (A). Log-rank test for survival comparison is shown in (B). Student's t test was used to compare gene expression levels in (D) and (E).

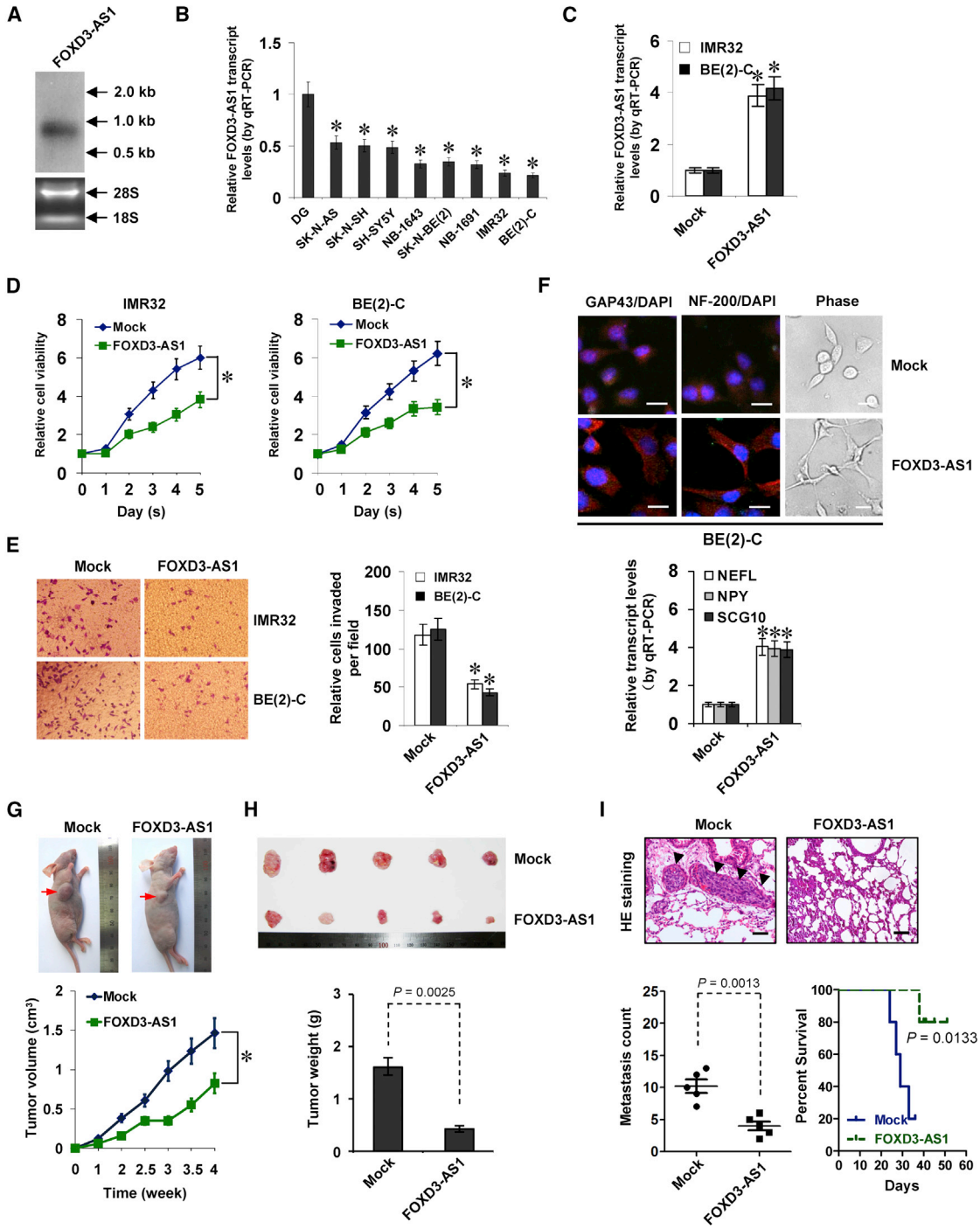

Figure 2. Ectopic Expression of *FOXD3-AS1* Leads to Suppression of NB Progression

(A) Northern blot (top) with a 310-bp specific probe indicating the existence of a 0.96-kb *FOXD3-AS1* transcript in total RNA (bottom) of SH-SY5Y cells. (B) Real-time qRT-PCR showing the *FOXD3-AS1* transcript levels (normalized to GAPDH) in normal dorsal ganglia (DG, n = 21) and NB cell lines. (C and D) Real-time qRT-PCR (C) and MTT colorimetric assay (D) depicting the change in FOXD3-AS1 expression (normalized to GAPDH) and cell viability (after culture for 1–5 days) of NB cells stably transfected with *FOXD3-AS1* compared with those transfected with empty vector (mock; mean ± SD, n = 5). (E) Representative images (left) and quantification (right) of a transwell Matrigel invasion assay (24 hr) indicating the invasion capability of NB cells stably transfected with mock or *FOXD3-AS1* (mean ± SD, n = 5). (F) Immunofluorescent confocal and phase images (top) showing the neuronal differentiation and neurite outgrowth of BE(2)-C cells stably transfected with mock or *FOXD3-AS1*, using the antibodies specific to neuronal markers GAP43 and NF-200. Scale bars, 10 μm. Real-time qRT-PCR (bottom) indicating the expression of established neuronal markers *NEFL*, *NPY*, and *SCG10*

(legend continued on next page)

FOXD3-AS1 overexpression (Figure 2F). Consistently, we observed a significant decrease in the growth rate and weight of xenografts formed by subcutaneous injection of NB cells stably transfected with *FOXD3-AS1* into nude mice (Figures 2G and 2H). In an experimental metastasis assay, athymic nude mice treated with tail vein injection of BE(2)-C cells stably transfected with *FOXD3-AS1* displayed fewer lung metastatic colonies and greater survival probability (Figure 2I). Together, these findings demonstrated that ectopic expression of *FOXD3-AS1* suppressed NB progression.

Nuclear FOXD3-AS1 Interacts with PARP1 Protein to Suppress Its Oncogenic Roles in NB Cells

To address the localization of FOXD3-AS1, we performed RNA-fluorescence *in situ* hybridization (RNA-FISH) and subcellular fractionation assays. The RNA-FISH assay revealed positive nuclear signals with intense dot-like structures in NB cells (Figure 3A) that were increased and decreased by ectopic expression or knockdown of *FOXD3-AS1*, respectively (Figure S2B). The subcellular fractionation assay indicated that in comparison to respective cytoplasmic glyceraldehyde 3-phosphate dehydrogenase (GAPDH) and nuclear (U1) controls, FOXD3-AS1 was enriched in the nuclear fraction (Figure 3A). To identify the protein partner and functional roles of FOXD3-AS1, biotin-labeled RNA pull-down was performed with subsequent mass spectrometry analysis in SH-SY5Y and BE(2)-C cells. For each cell line, differential protein pulled down by FOXD3-AS1 and FOXD3-AS1 antisense transcript was analyzed. Overlapping analysis of results from both cell lines revealed that PARP1 was the only consistent protein (with 73 detected peptides) pulled down by biotin-labeled FOXD3-AS1 (Figure 3B; Table S5). Western blot further validated that PARP1 was readily detected in the FOXD3-AS1 pull-down complex, but not in samples pulled down by FOXD3-AS1 antisense RNA or beads only (Figure 3B). The RNA immunoprecipitation (RIP) assay demonstrated an endogenous interaction between FOXD3-AS1 and PARP1 in BE(2)-C cells (Figure 3C). Deletion-mapping analyses indicated that exon 3 of *FOXD3-AS1* was essential for its interaction with PARP1 protein (Figure 3C). The *in vitro* binding assay indicated that the zinc finger (ZnF; 1–375 amino acids) or BRCA1 C terminus (BRCT)-tryptophan-glycine-arginine-rich (WGR; 376–662 amino acids) domain, but not the catalytic (CAT; 663–1,014 amino acids) domain, of glutathione S-transferase (GST)-tagged PARP1 protein was crucial for its interaction with FOXD3-AS1 (Figure 3D). Moreover, after transfection of FLAG-tagged *PARP1* truncates into BE(2)-C cells, the RIP assay indicated the essential roles of the ZnF or BRCT-WGR domain in interactions with FOXD3-AS1 (Figure 3E). Consistently, a RNA electrophoretic mobility shift assay (EMSA) using biotin-labeled probes (corresponding to exon 3) indicated the ability of the ZnF or BRCT-WGR domain of recombinant PARP1 protein to interact with FOXD3-AS1 (Figure 3F). The biological relevance of the interaction between FOXD3-AS1 and PARP1 protein was then examined. NB cells transfected with *PARP1* showed increased anchorage-independent growth and invasiveness (Figures 3G, 3H, and S2C), which was abolished by stable transfection of *FOXD3-AS1* (Figures 3G and 3H). Together, these results indicated that nuclear FOXD3-AS1 interacted with PARP1 protein to suppress its oncogenic roles in NB cells.

FOXD3-AS1 Represses the PARP1-Mediated PARylation of CTCF and Its Oncogenic Roles in NB Cells

To identify the PARP1 interacting protein affected by FOXD3-AS1, co-immunoprecipitation (co-IP) assay was performed using PARP1 antibody with subsequent mass spectrometry in SH-SY5Y and BE(2)-C cells stably transfected with empty vector (mock) or *FOXD3-AS1*. For each cell line, differential PARP1-interacting protein was analyzed between the mock and *FOXD3-AS1* transfection groups. Overlapping analysis of results from both cell lines revealed that CTCF (with 78 detected peptides) was the only FOXD3-AS1-affected nuclear protein pulled down by PARP1 antibody (Figure 4A; Table S6). Endogenous physical interaction and nuclear co-localization of PARP1 and CTCF were observed in BE(2)-C cells (Figures 4B and S2D). Co-IP and western blot assays demonstrated that the N terminus (1–291 amino acids), but not the ZnF domain (291–576 amino acids) or C terminus (576–727 amino acids), of Myc-tagged CTCF protein was essential for its interaction with PARP1 in BE(2)-C cells (Figure 4C). Meanwhile, the ZnF or BRCT-WGR domain of FLAG-tagged PARP1 protein was crucial for its interaction with CTCF (Figure 4D). Co-IP, western blot, and bimolecular fluorescence complementation (BiFC) assays indicated that ectopic expression or knockdown of *FOXD3-AS1* attenuated and facilitated the direct physical interaction between PARP1 and CTCF in NB cells, respectively (Figures S2E, 4E, and 4F). As shown in Figure 4G, *in vitro* incubation with *FOXD3-AS1* transcript decreased the amount of recombinant PARP1 protein pulled down by CTCF antibody and repressed the PARP1-mediated PARylation of CTCF (with a 180-kDa protein species as the predominant band). Notably, ectopic expression or knockdown of *FOXD3-AS1* decreased and increased the PARylation of CTCF, respectively (Figure 4H). Pretreatment of NB cells with PJ34, an established PARP1 inhibitor,[10] abolished the effects of *FOXD3-AS1* knockdown on PARylation of CTCF (Figure 4H). In addition, RIP and biotin-labeled RNA pull-down assays revealed no binding of FOXD3-AS1 to CTCF in NB cells (Figure S2F). Transfection of *CTCF* into NB cells resulted in its overexpression (Figure S2G) and increased anchorage-independent growth (Figure 4I) and invasiveness (Figure 4J). Meanwhile, transfection of *FOXD3-AS1* prevented NB cells from undergoing the changes in growth and invasion induced by ectopic expression

(normalized to GAPDH) in BE(2)-C cells stably transfected with mock or *FOXD3-AS1* (mean ± SD, n = 5). (G and H) Representative images (G, top), *in vivo* growth curve (G, bottom), and tumor weight at the endpoints (H) of xenografts formed by subcutaneous injection of BE(2)-C cells stably transfected with mock or *FOXD3-AS1* into the dorsal flanks of nude mice (n = 5 for each group) for 1 month. (I) Representative H&E staining images (top) and quantification (bottom left) of lung metastatic colonization and Kaplan-Meier curves (lower right) of nude mice treated with tail vein injection of BE(2)-C cells stably transfected with mock or *FOXD3-AS1* (n = 5 for each group). Student's t test and analysis of variance were used to analyze differences in (B)–(I). Log-rank test for survival comparison was used in (I). *$p < 0.01$ versus DG or mock.

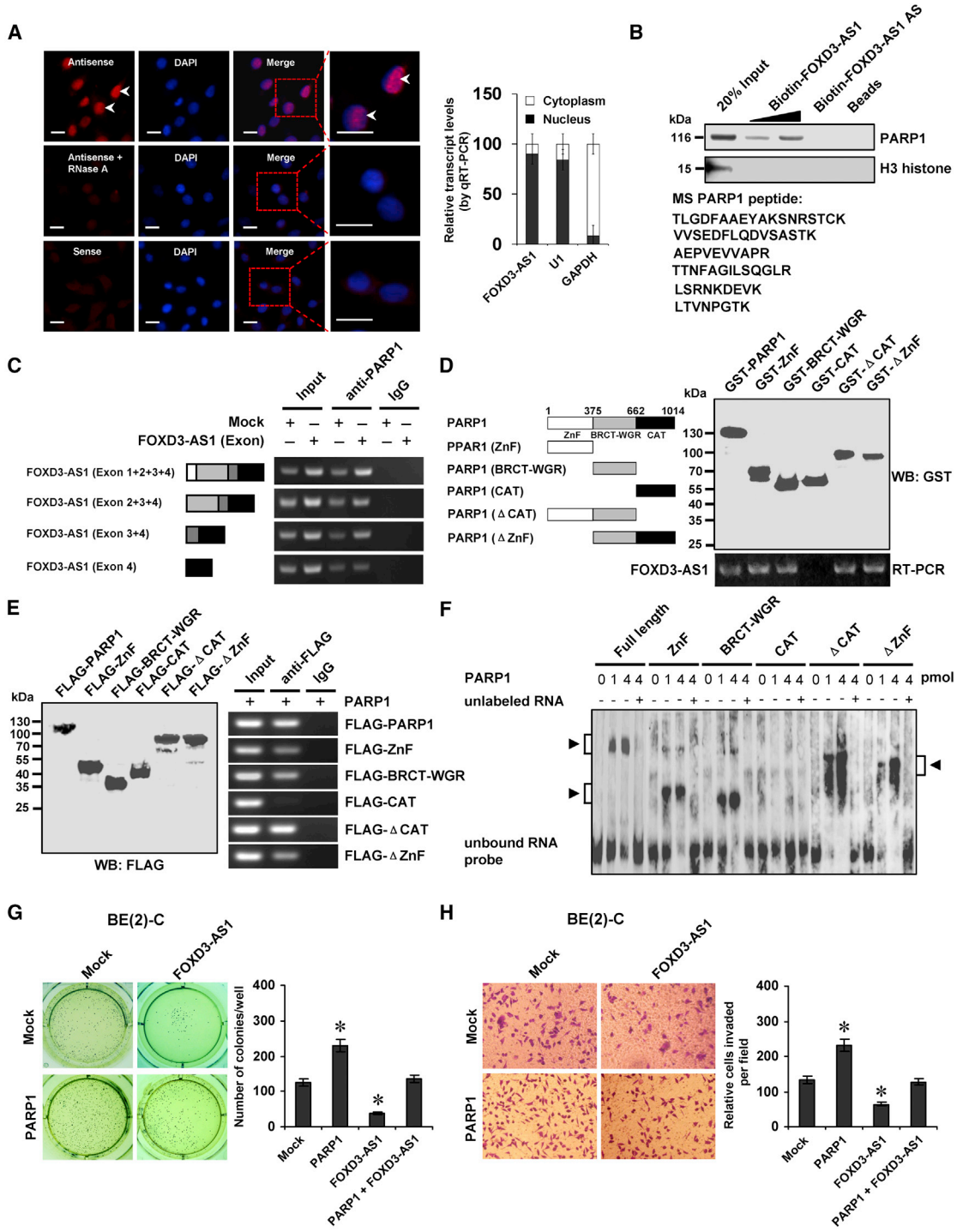

Figure 3. Nuclear FOXD3-AS1 Interacts with PARP1 Protein to Suppress Its Oncogenic Roles in NB Cells

(A) RNA fluorescence *in situ* hybridization images (left) showing the nuclear localization of FOXD3-AS1 in SH-SY5Y cells using a 310-bp antisense probe (red). A sense probe and antisense probe with RNase A (20 μg) treatment were used as negative controls. Scale bars, 10 μm. Real-time qRT-PCR (right) showing the distribution of FOXD3-AS1, U1, and GAPDH in subcellular fractions (mean ± SD, n = 4). (B) Biotin-labeled RNA pull-down (top) and mass spectrometry (MS) assay (bottom) showing the interaction between FOXD3-AS1 and PARP1 protein in SH-SY5Y cells. FOXD3-AS1 antisense (AS)- and bead-bound protein served as negative control. (C) RIP assay using PARP1 antibody indicating the interaction between FOXD3-AS1 and PARP1 protein in BE(2)-C cells transfected with a series of *FOXD3-AS1* truncates for 72 hr. IgG-bound RNA was

(legend continued on next page)

of *CTCF* (Figures 4I and 4J). Together, these results indicated that FOXD3-AS1 repressed the PARP1-mediated PARylation of CTCF and its oncogenic roles in NB cells.

FOXD3-AS1 Inhibits PARP1-Facilitated CTCF Activation and Facilitates the Expression of Tumor-Suppressive Genes in NB Cells

To identify the putative targets of FOXD3-AS1, we analyzed the genes consistently correlated ($p < 0.05$, FDR < 0.05) with FOXD3-AS1, PARP1, and CTCF in public datasets of 88 NB cases (GEO: GSE16476) and 64 neuroblastic tumors (GEO: GSE12460). Overlapping analysis ($p < 0.001$) of these genes and CTCF target genes in the ChIP-X database[11] revealed 76 potential downstream genes (Figure 5A). RNA sequencing (RNA-seq) revealed 1,542 upregulated and 1,650 downregulated genes (fold change > 2.0, $p < 0.05$) upon FOXD3-AS1 overexpression in BE(2)-C cells (Figure 5B). Based on overlapping analysis ($p < 0.001$) of results from public datasets (GEO: GSE16476 and GSE12460) and our RNA-seq data, 20 target genes of FOXD3-AS1 were identified (Figure 5B). Among them, the expression of forkhead box D3 (*FOXD3*), interferon induced protein with tetratricopeptide repeats 2 (*IFIT2*), interleukin-6 signal transducer (*IL6ST*), Kruppel-like factor 6 (*KLF6*), and sterile alpha motif domain containing 9 (*SAMD9*) was significantly correlated with that of FOXD3-AS1 (Figure S3A), PARP1 (Figure S4A), and CTCF (Figure S4B) in NB tissues and was associated with favorable outcome of patients (Figure S3B). Patients with high PARP1 ($p = 1.2 \times 10^{-3}$) or CTCF ($p = 9.0 \times 10^{-4}$) expression had lower survival probability (Figure S4C). To explore the roles of PARP1-mediated PARylation in regulating CTCF activity, a CTCF mutant (CTCF Mut) deficient in PARylation[12] was established, validated by IP and western blot assay (Figure S5A), and served as a dominant-negative control. Transfection of *CTCF* or *CTCF Mut* increased the enrichment of CTCF on the promoter of target genes *FOXD3*, *IFIT2*, *IL6ST*, *KLF6*, and *SAMD9* in BE(2)-C cells, which was not affected by treatment with PJ34 (Figure S5B). Notably, transfection of *CTCF* or *CTCF Mut* decreased and increased the transcript and protein levels of these downstream genes, respectively (Figures S5C and S5D). Treatment with PJ34 abolished the alteration in downstream gene expression induced by ectopic expression of *CTCF*, but not of *CTCF Mut* (Figures S5C and S5D). A dual-luciferase assay indicated the decreased *FOXD3* promoter activity in NB cells transfected with *CTCF* and mutation of the CTCF-binding site abolished these effects (Figure 5C). In addition, ectopic expression or knockdown of *FOXD3-AS1* abolished the decrease and increase of *FOXD3* promoter activity induced by overexpression or knockdown of *PARP1 or CTCF*, respectively (Figures 5C and S5E). Importantly, chromatin immunoprecipitation (ChIP) and qPCR indicated that overexpression or knockdown of *PARP1* or *CTCF* significantly altered the binding of CTCF, PARP1, enhancer of zeste homolog 2 (EZH2), histone H3 lysine 27 trimethylation (H3K27me3), and RNA polymerase II (RNA Pol II) to the promoters of the FOXD3-AS1 downstream genes *FOXD3*, *IFIT2*, *IL6ST*, *KLF6*, and *SAMD9*, which was rescued by ectopic expression or knockdown of *FOXD3-AS1*, respectively (Figures 5D and S6). Real-time qRT-PCR and western blot indicated that ectopic expression or knockdown of *FOXD3-AS1* prevented the NB cells from transcriptional repression or activation of CTCF target genes induced by ectopic expression or knockdown of *PARP1* or *CTCF* (Figures 5E and S7). Collectively, these data demonstrated that FOXD3-AS1 inhibited PARP1-facilitated CTCF activation and facilitated the expression of tumor-suppressive genes in NB cells.

FOXD3-AS1 Harbors Tumor-Suppressive Properties by Repressing Oncogenic Roles of PARP1 and CTCF

The functional interplay of FOXD3-AS1, PARP1, and CTCF was then investigated in cultured SH-SY5Y cells with high FOXD3-AS1 levels. Stable knockdown of *FOXD3-AS1* facilitated the anchorage-independent growth of NB cells (Figure 6A). Since PARP1 and CTCF are involved in the repair of DNA damage,[13,14] the roles of FOXD3-AS1 in this process were further investigated. Western blot and flow cytometry assays showed that knockdown of *PARP1* or *CTCF* led to increased levels of phosphorylated H2AX (γH2AX) and RAD51 (Figure S8A), markers for DNA damage and homologous recombination repair, and facilitated the cisplatin-induced DNA damage and apoptosis in NB cells (Figures S8A and S8B). Meanwhile, knockdown of *FOXD3-AS1* attenuated these changes in DNA damage and cell apoptosis induced by cisplatin or transfection of sh-PARP1 #2 or sh-CTCF #1 (Figures S8A and S8B). In addition, knockdown of *FOXD3-AS1* decreased the expression of established neuronal differentiation markers neurofilament light chain (*NEFL*), neuropeptide Y (*NPY*), and superior cervical ganglia-10 (*SCG10*)[7] (Figure S8C) and suppressed the GAP43- and NF-200-positive neuronal differentiation (Figure S8D). In a Matrigel invasion assay, NB cells stably transfected with sh-FOXD3-AS1 showed increased invasiveness (Figure 6B). Knockdown of *PARP1* or *CTCF* prevented NB cells from undergoing the changes in growth, differentiation, and invasion induced by stable knockdown of *FOXD3-AS1* (Figures 6A, 6B, S8C, and S8D). In a mouse xenograft tumor assay, stable knockdown of *FOXD3-AS1* into SH-SY5Y cells resulted in increased growth, tumor weight, and the Ki-67-positive rate of subcutaneous xenograft tumors (Figures 6C– 6E) and led to significantly more lung metastatic colonies and lower survival probability in athymic nude mice (Figures 6F and 6G). Meanwhile, knockdown of *PARP1* or *CTCF* attenuated

taken as negative control. (D) *In vitro* binding assay depicting the recovered FOXD3-AS1 levels by RIP (bottom) after incubation with full-length and truncates of GST-tagged recombinant PARP1 protein validated by western blot (top). (E) Western blot (left) and RIP (right) assays indicating the interaction between FOXD3-AS1 and PARP1 protein in BE(2)-C cells transfected with a series of FLAG-tagged *PARP1* truncates for 72 hr. (F) RNA EMSA determining the interaction between recombinant PARP1 protein and biotin-labeled RNA probe for *FOXD3-AS1* (arrowheads), with or without competition using an excess of unlabeled homologous RNA probe. (G and H) Representative images (left) and quantification (right) of soft agar (G) and transwell Matrigel invasion (H) assays indicating the anchorage-independent growth (21 days) and invasion (24 hr) capability of NB cells stably transfected with mock or *PARP1* and those co-transfected with *FOXD3-AS1* (mean ± SD, n = 5). Student's t test was used to analyze differences in (G) and (H). *$p < 0.01$ versus mock.

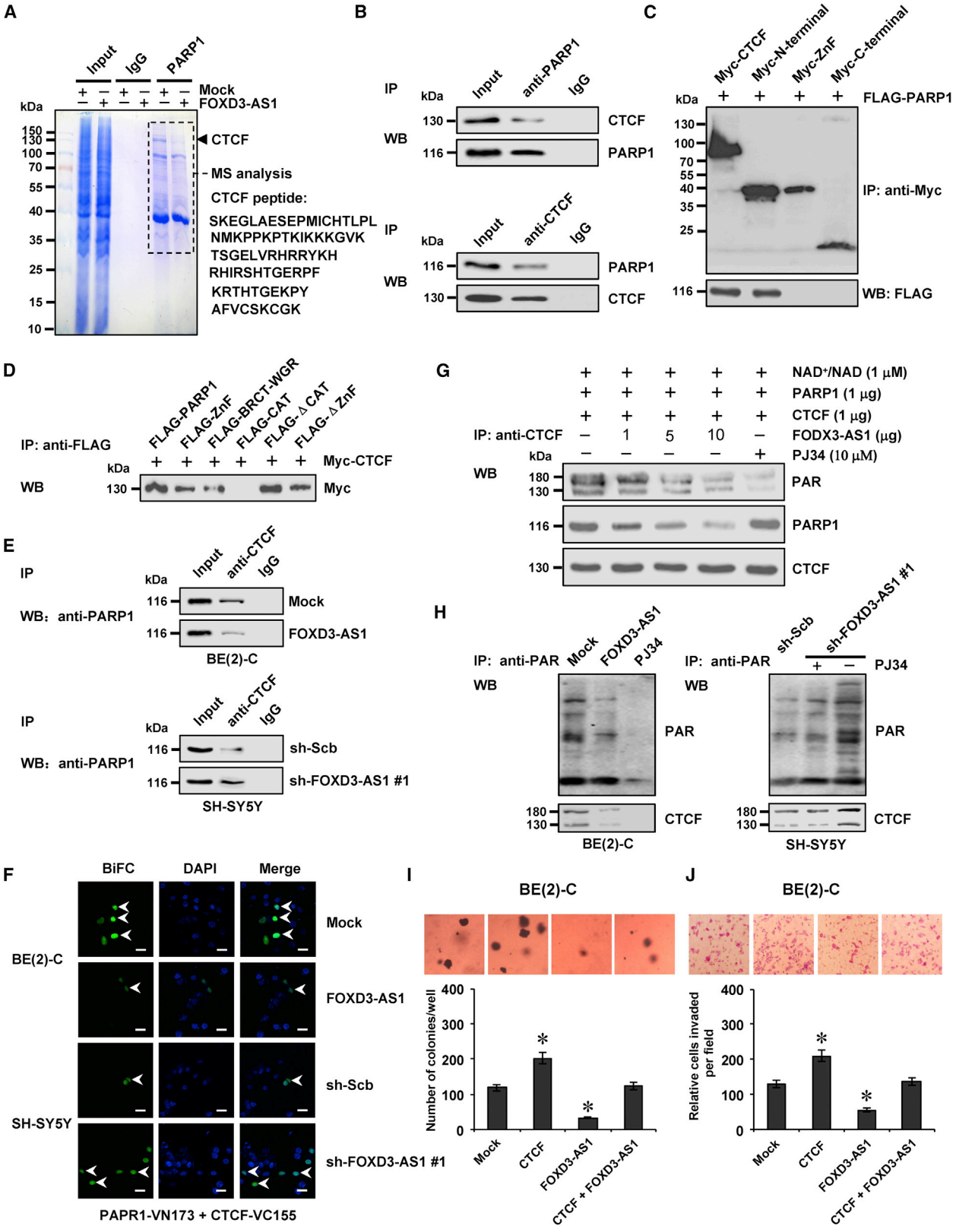

(legend on next page)

the impacts of *FOXD3-AS1* depletion on tumor growth and metastasis of NB cells *in vivo* (Figures 6C–6G). These results suggested that FOXD3-AS1 harbors tumor-suppressive properties by repressing the oncogenic roles of PARP1 or CTCF *in vitro* and *in vivo*.

Therapeutic Efficiencies of *FOXD3-AS1* Construct and siRNAs for *PARP1* or *CTCF In Vivo*

We further explored the therapeutic efficiencies of *FOXD3-AS1* construct and siRNAs specific for *PARP1* and *CTCF* (si-PARP1 and si-CTCF) on tumor growth and survival in athymic nude mice bearing xenografts. Fourteen days after tumor implantation, mice were randomized into treatment groups, and *FOXD3-AS1*, si-PARP1 or si-CTCF was administered by standard intratumoral injection (Figure 7A). Administration of *FOXD3-AS1*, si-PARP1, or si-CTCF significantly reduced the volume and weight of xenograft tumors formed by hypodermic injection of BE(2)-C cells when compared to those treated with empty vector (mock) or scramble siRNA (si-Scb; Figures 7A and 7B). Meanwhile, the body weights of nude mice (indicating the tumor burden) were increased in *FOXD3-AS1*, si-PARP1, or si-CTCF treatment groups more than those treated with mock or si-Scb (Figure 7C). In addition, Kaplan-Meier survival analysis revealed that administration of *FOXD3-AS1*, si-PARP1, or si-CTCF prolonged the survival time of nude mice (Figure 7D). Real-time qRT-PCR indicated that administration of *FOXD3-AS1*, si-PARP1, or si-CTCF increased FOXD3-AS1 levels and decreased the expression of PARP1 and CTCF within tumors, respectively, with corresponding changes in downstream gene expression levels (Figure 7E). These results indicated the therapeutic efficiencies of *FOXD3-AS1* construct and siRNAs for *PARP1* and *CTCF* in nude mice bearing xenograft tumors.

Inducible FOXD3-AS1 Plays Crucial Roles in Retinoic-Acid-Facilitated Differentiation and Tumor Suppression in NB Cells

ChIP sequencing (ChIP-seq) datasets derived from the UCSC Genome Browser indicated the presence of a retinoid X receptor alpha (RXRα) peak in the *FOXD3-AS1* promoter region (Figure S9A). Treatment of NB cells with all-*trans* retinoic acid (ATRA) resulted in increased expression of FOXD3-AS1, while transfection of sh-FOXD3-AS1 abolished these effects (Figure 8A). However, ectopic expression of *MYCN* did not affect FOXD3-AS1 levels in NB cells (Figure S9B). ChIP and qPCR using tiled primer sets revealed endogenous binding of RXRα to the −293/−62 region, but not the −716/−537 region, of the *FOXD3-AS1* promoter in IMR32 and BE(2)-C cells (Figure 8B). ATRA treatment resulted in increased enrichment of RXRα on the *FOXD3-AS1* promoter, which was abolished by knockdown of *RXRα* in NB cells (Figures 8C and S9C). Dual-luciferase reporter arrays indicated that ATRA facilitated *FOXD3-AS1* promoter activity in IMR32 and BE(2)-C cells, which was abolished by mutation of the RXRα-binding site located at −268/−265 bp or knockdown of *RXRα* (Figure 8D). Moreover, ATRA treatment induced differentiation and attenuated the *in vitro* anchorage-independent growth and invasion capacity of NB cells, which were abolished by stable knockdown of *FOXD3-AS1* (Figures S9D, 8E, and 8F). These results indicated that inducible FOXD3-AS1 plays crucial roles in retinoic-acid-facilitated differentiation and tumor suppression in NB cells.

DISCUSSION

In this study, we identify the risk-associated lncRNA FOXD3-AS1 as an independent prognostic marker for progression and favorable outcome of NB. Our expression profiles and functional and mechanistic data indicate that FOXD3-AS1 is underexpressed in NB tissues with clinical progression, advanced stages, or poor outcome. We demonstrate that as a nuclear lncRNA, FOXD3-AS1 interacts with PARP1 protein to repress the activation of CTCF, resulting in derepressed expression of downstream tumor-suppressive genes (Figure S10). Our cell culture and mouse xenograft models clearly demonstrate that FOXD3-AS1 possesses tumor-suppressive properties by repressing the oncogenic roles of PARP1 or CTCF, such as promotion of neuronal differentiation and suppression of growth, invasion, and metastasis of NB cells. Similarly, previous studies show that lncRNA NBAT1 exerts tumor-suppressive roles by activating the RE1 silencing transcription factor,[4] indicating the essential role of tumor-suppressive lncRNAs in NB progression. Interestingly, recent work shows that FOXD3-AS1 is highly expressed in high-grade glioma and associated with lower survival probability, while knockdown of *FOXD3-AS1* reduces FOXD3 expression and suppresses the growth and aggressiveness of malignant glioma cells.[15] In hyperoxia/reactive-oxygen-species-induced lung injury, FOXD3-AS1 is upregulated to induce lung epithelial cell death by acting as a sponge

Figure 4. FOXD3-AS1 Represses the PARP1-Mediated PARylation of CTCF and Its Oncogenic Roles in NB Cells

(A) Immunoprecipitation (IP) (left) and mass spectrometry (MS) assay of indicated electrophoretic bands (right) showing the changes in PARP1-interacting protein in BE(2)-C cells stably transfected with empty vector (mock) or *FOXD3-AS1*. (B) Co-IP and western blot revealing the endogenous interaction between PARP1 and CTCF in the BE(2)-C cells. IgG-bound protein was taken as negative control. (C) Co-IP and western blot showing the interaction between PARP1 and CTCF in the BE(2)-C cells co-transfected with FLAG-tagged *PARP1* and a series of Myc-tagged *CTCF* truncates for 72 hr. (D) Co-IP and western blot indicating the interaction between PARP1 and CTCF in SH-SY5Y cells transfected with FLAG-tagged *PARP1* truncates and Myc-tagged *CTCF* vector for 72 hr. (E) Co-IP and western blot revealing the interaction between PARP1 and CTCF in BE(2)-C and SH-SY5Y cells stably transfected with mock, *FOXD3-AS1*, sh-Scb, or sh-FOXD3-AS1 #1. (F) Bimolecular fluorescence complementation (BiFC) vectors pBiFC-PARP1-VN173 and pBiFC-CTCF-VC155 were co-transfected into BE(2)-C and SH-SY5Y cells stably transfected with mock, *FOXD3-AS1*, sh-Scb, or sh-FOXD3-AS1 #1. 24 hr later, direct interaction between PARP1 and CTCF within tumor cells was observed under a confocal microscope. Scale bars, 10 μm. (G) IP and western blot assays indicating the recombinant PARP1 and CTCF protein pulled down by CTCF antibody with *in vitro* incubation with NAD^+/NAD, FOXD3-AS1, and PARP1 inhibitor (PJ34) for 24 hr. (H) IP and western blot assay indicating the expression of PARylated CTCF in NB cells stably transfected with mock, *FOXD3-AS1*, sh-Scb, or sh-FOXD3-AS1 #1, and those treated with PJ34 (10 μmol/L) for 24 hr. (I) and (J) Representative images (top) and quantification (bottom) of soft agar (I) and transwell Matrigel invasion (J) assays indicating the anchorage-independent growth (21 days) and invasion (24 hr) capability of NB cells stably transfected with mock or *CTCF* and those co-transfected with *FOXD3-AS1* (mean ± SD, n = 5). Student's t test was used to analyze differences in in (I) and (J). *$p < 0.01$ versus mock.

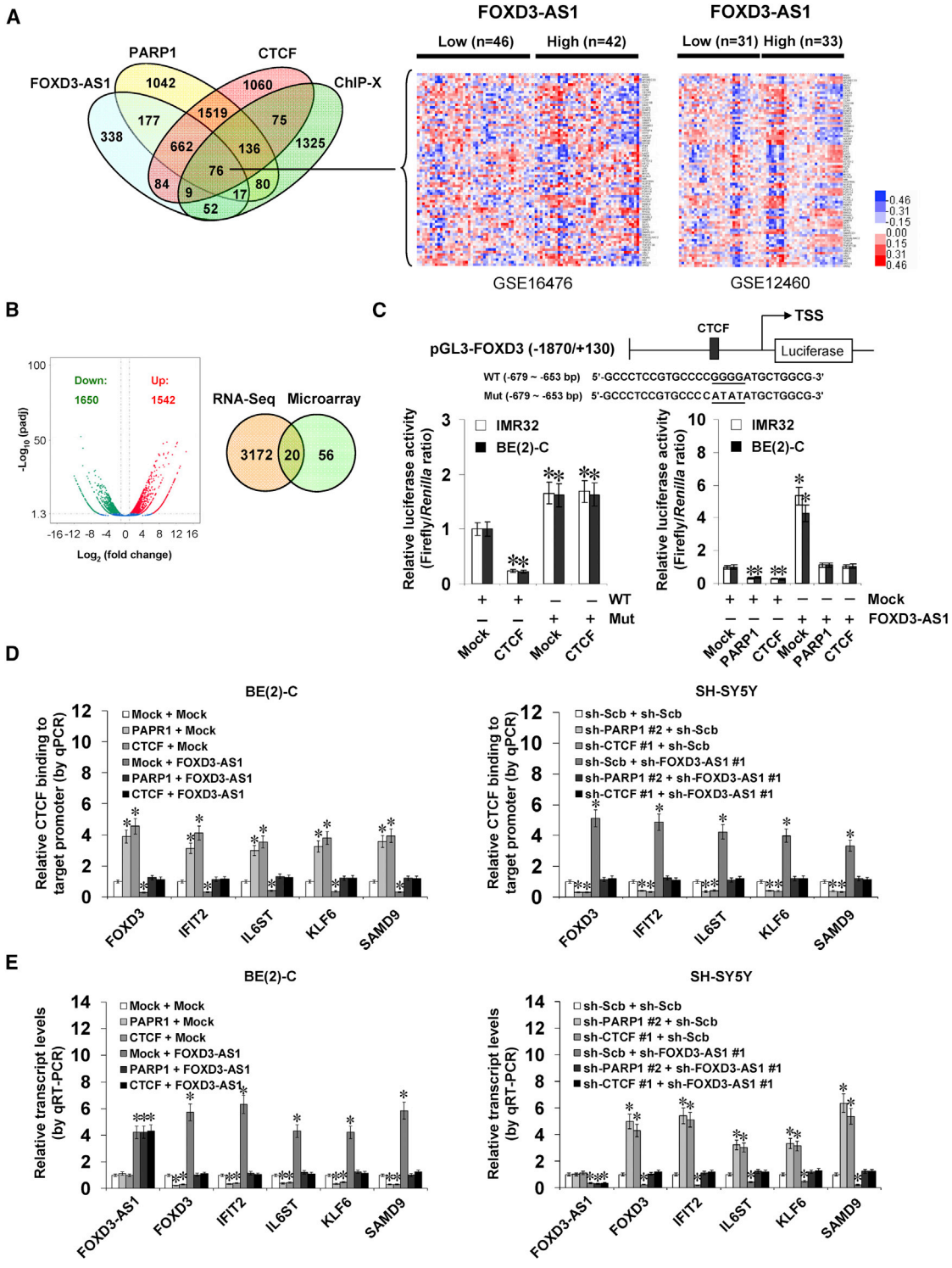

Figure 5. FOXD3-AS1 Inhibits the PARP1-Facilitated CTCF Activation and Facilitates the Expression of Tumor Suppressive Genes in NB Cells

(A) Venn diagram (left) and heatmap (right) showing the CTCF target genes consistently correlated ($p < 0.05$, FDR < 0.05) with FOXD3-AS1, PARP1, and CTCF in public datasets (GEO: GSE16476 and GSE12460) and ChIP-X databases. (B) Volcano plots (left) derived from RNA-seq revealing the alteration of gene expression (fold change > 2.0, $p < 0.05$) in BE(2)-C cells stably transfected with empty vector (mock) or *FOXD3-AS1*. Venn diagram (right) indicating further intersection of CTCF target genes (A) and those differently expressed in RNA-seq. (C) Dual-luciferase assay indicating the relative activity (24 hr post-transfection) of *FOXD3* promoter reporter with wild-type

(legend continued on next page)

for miR-150.[16] In line with these studies, our evidence showed that FOXD3-AS1 was positively correlated with its parental coding gene, *FOXD3*, and exerted a slight apoptosis-inducing effect in NB cells. We believe that FOXD3-AS1 may play crucial roles in non-cancerous physiological conditions and exert oncogenic or tumor-suppressive functions in a context-dependent manner.

As a major member of the PARP family, PARP1 is able to catalyze the covalent attachment of PAR moieties on target nuclear proteins from donor nicotinamide adenine dinucleotide (NAD^+) molecules[17] and plays crucial roles in modulating DNA repair, genomic integrity, and gene transcription.[18–20] PARP1 is activated by and facilitates the repair of DNA-base damage and single-strand breaks.[13] High levels and activity of PARP1 are correlated with cancer progression.[21] For example, PARP-1 induces the PARylation of tumor suppressor p53 to block the expression of metastasis-associated protein 1 in cancer cells.[21] PARP1 mediates the PARylation of snail family transcriptional repressor 1 and SMAD family member 3/4 to regulate the epithelial-to-mesenchymal transition process.[22,23] It has been established that PARP1 inhibitors are useful in combination with chemotherapy and radiotherapy or as single therapeutic agents for cancers defective in homologous recombination.[13] Recent evidence shows that PARP1 regulates the apoptosis of lung cancer cells through physical interaction with Lnc_bc060912, a lncRNA repressed by p53.[24] In addition, PARP1 interacts with noncoding telomeric-repeat-containing RNA to stimulate the senescence-associated secretory phenotype in fetal lung fibroblast cells,[25] indicating that PARP1 has an intrinsic ability to bind RNA. In this study, the lncRNA FOXD3-AS1 was identified as a RNA partner interacting with PARP1 protein. Mechanistically, FOXD3-AS1 physically interacts with the ZnF or BRCT-WGR domain of PARP1 protein to inhibit the PARP1-mediated PARylation and activation of CTCF, suggesting a role for FOXD3-AS1 in repressing active PARP1-CTCF transcriptional complexes.

CTCF is a highly conserved and ubiquitously expressed nuclear protein that regulates gene expression via combinatorial use of its 11 ZnF domains in a context-dependent fashion.[26] CTCF binds to the promoter of genes involved in cancer, such as *c-Myc*, *p53*, retinoblastoma, $p16^{INK4a}$, and telomerase reverse transcriptase, and regulates their expression through epigenetic mechanisms.[27] CTCF preserves promoter chromatin organization via recruiting EZH2 and maintaining repressive mark H3K27me3.[28] Loss of heterozygosity or mutation at the *CTCF* locus has been found in different malignancies.[29] However, studies have shown that elevated CTCF expression in breast and lung cancer cells is associated with apoptosis resistance,[30,31] and knockdown of *CTCF* leads to apoptotic cell death in breast cancer cells,[30] indicating the oncogenic roles of CTCF in tumorigenesis. Our previous studies have indicated that CTCF is an independent predictor of unfavorable outcome in NB patients.[7] In this study, we demonstrated that CTCF induced epigenetic inactivation of downstream target genes by recruiting repressive histone marks and attenuating the enrichment of RNA Pol II. These CTCF target genes, such as *FOXD3*,[32,33] *IFIT2*,[34] *IL6ST*,[35] *KLF6*,[36] and *SAMD9*,[37] are associated with tumor proliferation, neuronal differentiation, invasion, and metastasis. The consistent association between expression of these genes and patient survival in public datasets further supports their functional roles in NB progression. Since depletion of *CTCF* abolished the changes in biological features of NB cells induced by *FOXD3-AS1* knockdown, our findings indicate that the tumor-suppressive functions of FOXD3-AS1 are mediated, at least in part, by regulating the CTCF activity.

The functions of CTCF are regulated by post-translational modifications, such as phosphorylation, SUMOylation, and PARylation.[26] In particular, CTCF forms functional complexes with PARP1 and is able to induce PARP1 activity in the absence of DNA damage.[38] In turn, PARP1 mediates the covalent PARylation of CTCF, resulting in a CTCF protein of 130 kDa (CTCF-130) and 180 kDa (CTCF-180) that contains several or more than 20 ADP-ribose residues, respectively.[12] Previous studies have shown that inhibition of PARylation impairs the effects of CTCF on nucleolar transcription.[39] PARylation is also required for optimal CTCF function in transcriptional activation of *p19ARF* promoter and inhibition of cell proliferation.[12] Recent evidence shows that CTCF participates in the DNA damage response via PARylation, and CTCF-deficient cells are hypersensitive to genotoxic stress.[14] In this study, we demonstrate that PARP1-mediated PARylation is pivotal for maintaining the functions of CTCF in repressing transcription of target genes in NB cells. As an inhibitor of PARP1-mediated PARylation of CTCF, FOXD3-AS1 is potentially involved in regulating DNA damage repair and increasing sensitivity to chemotherapeutic agents. Since similar domains of PARP1 are involved in its interaction with CTCF or FOXD3-AS1, we suspect that FOXD3-AS1 may interfere with the structure and domain utilization of PARP1, which warrants our further investigation.

Retinoic acid, an active metabolite of vitamin A, is a well-accepted signaling molecule involved in embryonic neurogenesis, neural differentiation, and cell fate determination.[40] ATRA regulates the transcription of target genes by binding to heterodimer of retinoid alpha receptor and RXR.[40] Previous studies have shown that ATRA induces the expression of HOXA antisense RNA 2, which in turn suppresses ATRA-induced apoptosis of leukemia cells.[41] In addition,

(WT) or mutant (Mut) CTCF-binding site (left) in NB cells transfected with mock or *CTCF* and that of *FOXD3* promoter reporter with a wild-type CTCF binding site in tumor cells stably transfected with mock, *FOXD3-AS1*, *PARP1*, or *CTCF* (mean ± SD, n = 5). (D) ChIP and qPCR assay showing the enrichment of CTCF on target gene promoters (normalized to input DNA) in BE(2)-C and SH-SY5Y cells stably transfected with mock, *FOXD3-AS1*, sh-Scb, or sh-FOXD3-AS1 #1 and those co-transfected with *PARP1*, *CTCF*, sh-PARP1 #2, or sh-CTCF #1 (mean ± SD, n = 5). (E) Real-time qRT-PCR indicating the differential transcript levels of CTCF target genes *FOXD3*, *IFIT2*, *IL6ST*, *KLF6*, and *SAMD9* (normalized to GAPDH) in NB cells stably transfected with mock, *FOXD3-AS1*, sh-Scb, or sh-FOXD3-AS1 #1 and those co-transfected with *PARP1*, *CTCF*, sh-PARP1 #2, or sh-CTCF #1 (mean ± SD, n = 5). Student's t test was used to analyze differences in (C)–(E). *$p < 0.01$ versus mock+WT, mock, or sh-Scb.

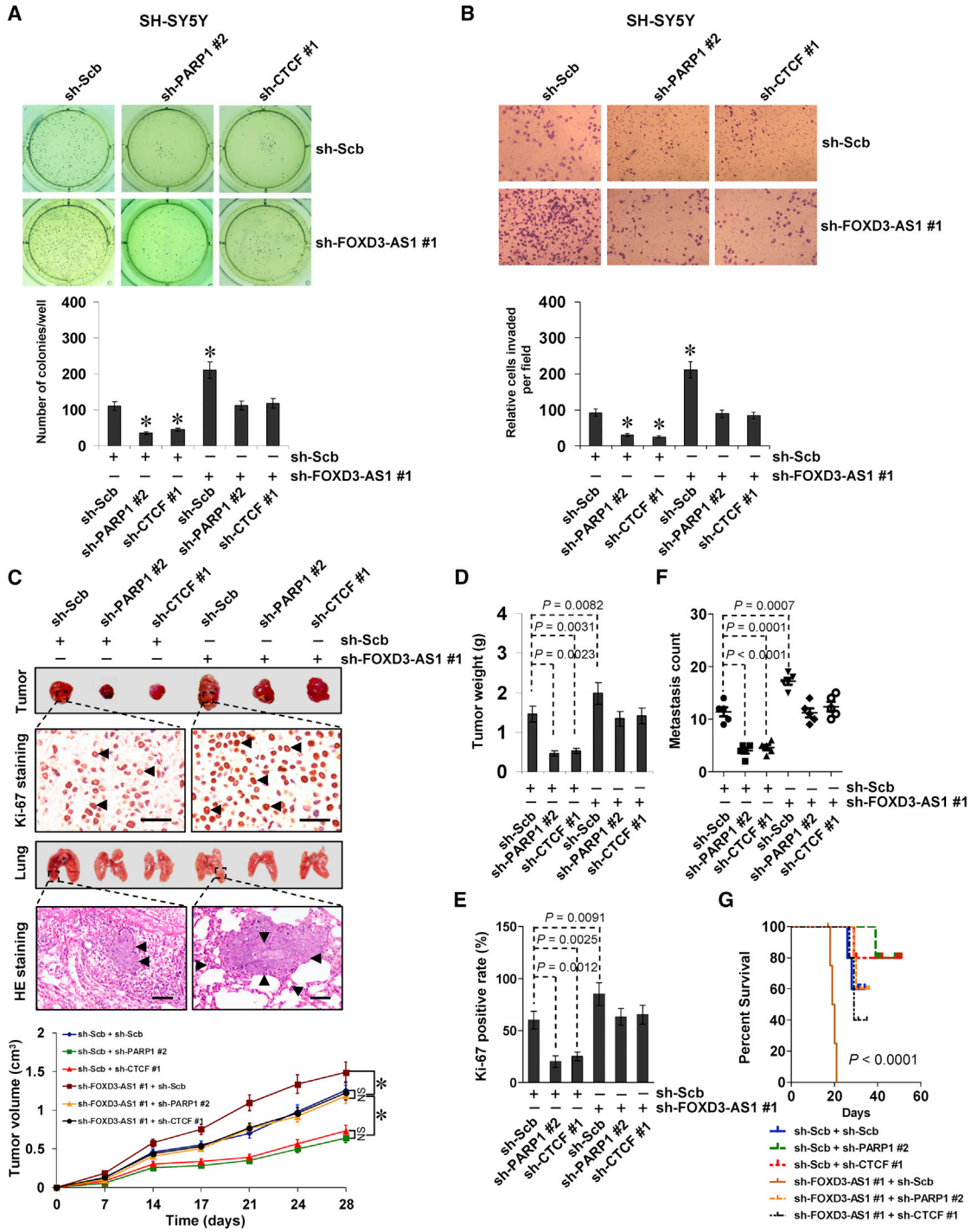

Figure 6. FOXD3-AS1 Harbors Tumor-Suppressive Properties by Repressing Oncogenic Roles of PARP1 and CTCF

(A and B) Representative images (top) and quantification (bottom) of soft agar (A) and transwell Matrigel invasion (B) assays indicating the anchorage-independent growth (for 21 days) and invasion (for 24 hr) capability of NB cells stably transfected with sh-Scb or sh-FOXD3-AS1 #1 and those co-transfected with sh-PARP1 #2 or sh-CTCF #1 (mean ± SD, n = 6). (C–G) Representative images (C, top), *in vivo* growth curve (C, bottom), tumor weight (D), and Ki-67-positive rate (E) at the endpoints of xenografts in athymic nude mice formed by hypodermic injection of SH-SY5Y cells stably transfected with sh-Scb or sh-FOXD3-AS1 #1 and those co-transfected with sh-PARP1 #2 or

(legend continued on next page)

ATRA induces the expression of nuclear paraspeckle assembly transcript 1 (NEAT1) during differentiation of leukemia cells, and knockdown of *NEAT1* blocks ATRA-induced differentiation.[42] In this study, our findings indicated that ATRA induced the expression of FOXD3-AS1 through transcription factor RXRα, and knockdown of *FOXD3-AS1* abolished ATRA-induced differentiation and inhibition of aggressiveness of NB cells, indicating the potential roles of FOXD3-AS1 in the retinoic acid/RXRα signaling that regulates NB progression.

In summary, we have demonstrated that the lncRNA FOXD3-AS1 is downregulated and serves as an independent prognostic factor for favorable outcome of NB. FOXD3-AS1 directly interacts with PARP1 to inhibit the PARylation and activation of CTCF. Depletion of *FOXD3-AS1* is essential for suppressing the neuronal differentiation and maintaining the growth, invasion, and metastasis of NB cells *in vitro* and *in vivo*. Treatment with *FOXD3-AS1* construct or siRNAs against *PARP1* or *CTCF* reduces tumor growth and prolongs the survival time of nude mice bearing xenografts. In addition, inducible FOXD3-AS1 plays crucial roles in the all-*trans*-retinoic-acid-mediated therapeutic effects on NB. This study extends our knowledge of a crucial lncRNA associated with NB progression and suggests that FOXD3-AS1, PARP1, and CTCF may serve as potential targets for clinical therapeutics of NB.

MATERIALS AND METHODS

Cell Culture

Human *MYCN*-amplified (NB-1643, SK-N-BE(2), NB-1691, IMR32, and BE(2)-C) and non-*MYCN*-amplified (SK-N-AS, SH-SY5Y, and SK-N-SH) NB cell lines were obtained from the Type Culture Collection of Chinese Academy of Sciences (Shanghai, China) and American Type Culture Collection (Rockville, MD). Cell lines were authenticated by the provider, used within 6 months after resuscitation of frozen aliquots, and grown in RPMI 1640 medium (Life Technologies, Gaithersburg, MD) supplemented with 10% fetal bovine serum (Life Technologies), penicillin (100 U/mL), and streptomycin (100 μg/mL). Cells were incubated in serum-free RPMI 1640 for 4 hr and treated with PJ34 (Sigma, St. Louis, MO) or ATRA (Sigma) as indicated.

Northern Blot

The 310-bp probe was generated using the PCR DIG Probe Synthesis Kit (Roche, Indianapolis, IN) with the primer set indicated in Table S7. For northern blot, 20 μg total RNA was separated on 3-(N-morpholino)propanesulfonic acid (MOPS)-buffered 2% (w/v) agarose gel containing 1.2% (v/v) formaldehyde under denaturing conditions for 4 hr at 80 V and transferred to Hybond-N+ membrane (Pall, Port Washington, NY). Prehybridization was carried out at 65°C for 30 min in DIG Easy Hyb solution (Roche). Hybridizations were performed at 65°C for 16–18 hr. Blots were washed stringently, detected by anti-digoxigenin (DIG) antibody staining, and recorded on X-ray films with the chemiluminescence substrate CSPD (Roche).[43]

Gene Set Enrichment Analysis

Gene set enrichment analysis was performed as previously described.[44] Published gene sets were used as indicated. Datasets were generated from published microarray (GEO: GSE16476) results.

RACE Assay

To characterize the 5′ and 3′ ends of *FOXD3-AS1*, total RNA extracted from SH-SY5Y cells was used to generate RACE-ready cDNA, and PCR was performed according to the manual of SMARTer RACE cDNA Amplification Kit (Clontech Laboratories, Mountain View, CA). cDNA ends were amplified with universal primer mix and gene-specific primers (Table S7).

RNA-FISH Assay

Cells were seeded on coverslips and fixed with 4% paraformaldehyde. Biotin-labeled antisense and sense RNA probes for *FOXD3-AS1* were *in vitro* transcribed with Biotin RNA Labeling Mix (Roche, Indianapolis, IN) and T7 RNA polymerase. Hybridization was carried out in a humidified chamber at 37°C for 16 hr, with or without RNase A (20 μg) treatment. Cells were incubated with streptavidin-conjugated Cy3 and counterstained with DAPI.

Gene Overexpression and Knockdown

Human *FOXD3-AS1* cDNA (963 bp), *PARP1* cDNA (3,045 bp), and *CTCF* cDNA (2,184 bp) and their truncations were amplified from NB tissue (Table S8) and subcloned into pcDNA3.1 (Invitrogen, Carlsbad, CA), pCMV-3Tag-1C (Addgene, Cambridge, MA), and pCMV-N-Myc (Beyotime Biotechnology, Haimen, China), respectively. Mutation of the CTCF PARylation site was performed with the GeneTailor Site-Directed Mutagenesis System (Invitrogen) and PCR primers (Table S8). Oligonucleotides encoding short hairpin RNAs (shRNAs) specific for *FOXD3-AS1*, *PARP1*, *CTCF*, or *RXRα* (Table S9) were subcloned into GV102 (Genechem, Shanghai, China). Stable cell lines were screened by administration of neomycin or puromycin (Invitrogen). Empty vector and scramble shRNA (sh-Scb) were applied as controls (Table S9).

RNA-Seq Assay

Total RNA of 1×10^6 cells was isolated using TRIzol reagent (Life Technologies). Library preparation and transcriptome sequencing on an Illumina HiSeq X Ten platform were performed by Novogene Bioinformatics Technology (Beijing, China), and 100-bp paired-end reads were generated. HTSeq v0.6.0 was used to count the read numbers mapped to each gene, and fragments per kilobase of transcript per million fragments mapped (FPKM) of each gene were

sh-CTCF #1 (n = 5 for each group). Representative images (C, top), H&E staining (C, arrowheads), quantification (F) of lung metastatic colonies, and Kaplan-Meier curves (G) of athymic nude mice (n = 5 for each group) with tail vein injection of SH-SY5Y cells stably transfected with sh-Scb or sh-FOXD3-AS1 #1 and those co-transfected with sh-PARP1 #2 or sh-CTCF #1. Scale bars, 100 μm. Student's t test and analysis of variance were used to analyze differences in (A)–(F). Log-rank test for survival comparison was used in (G). *p < 0.01 versus sh-Scb. NS, not significant.

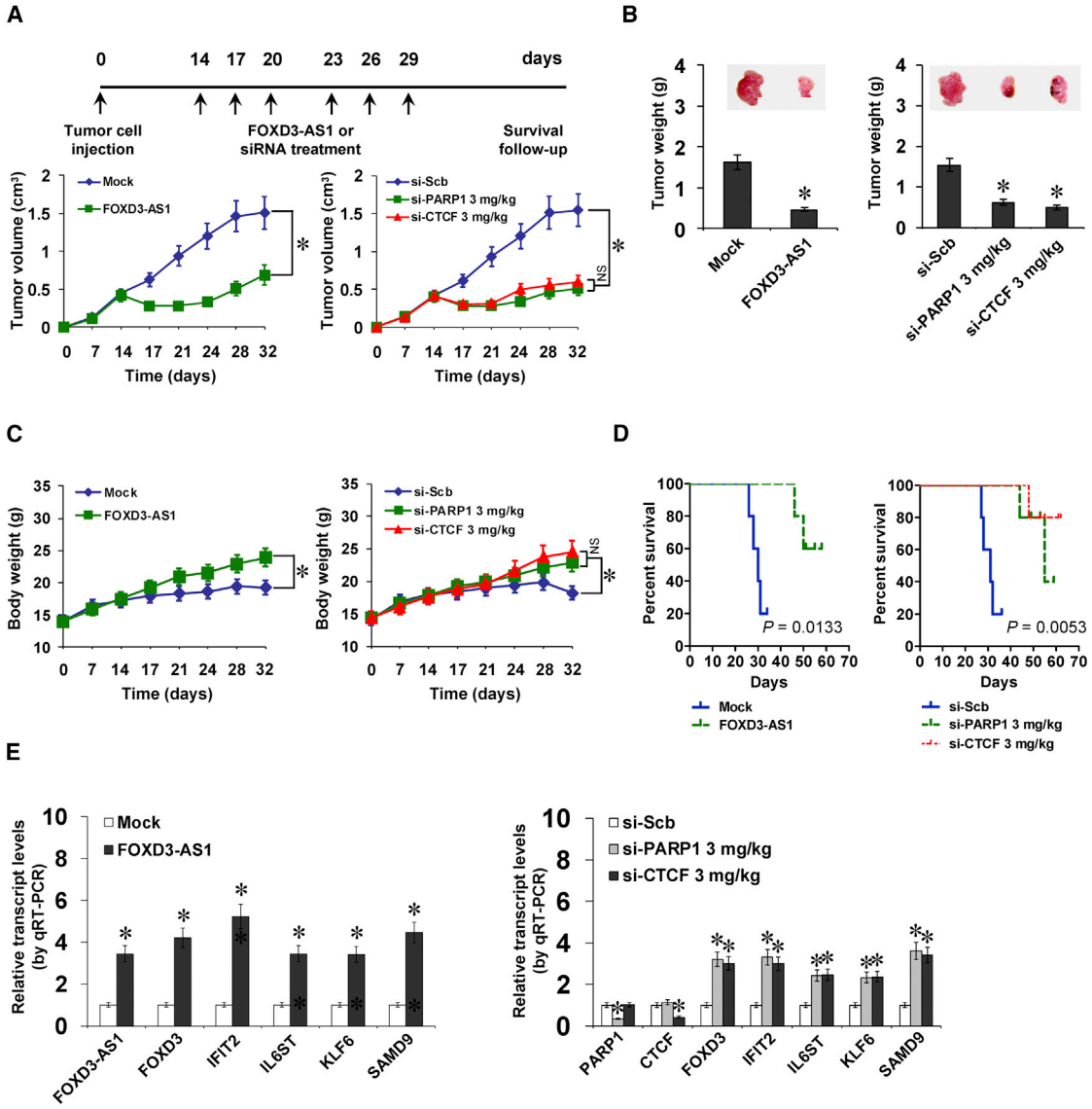

Figure 7. Therapeutic Efficiencies of *FOXD3-AS1* Construct and siRNAs for *PARP1* or *CTCF In Vivo*

(A–D) Viable BE(2)-C cells (1×10^6) were injected subcutaneously into the right flank of nude mice. Two weeks after tumor cell inoculation with confirmation of successful maturation of tumors, mice were divided randomly into groups (n = 5 for each group) and treated by intratumoral injection of empty vector (mock), *FOXD3-AS1*, scramble siRNA (si-Scb), si-PARP1, or si-CTCF (3 mg/kg; A, top). The *in vivo* growth curve (A, bottom), tumor weight (B), and body weight (C) and Kaplan-Meier curves (D) of nude mice were monitored (mean ± SD, n = 5). (E) Real-time qRT-PCR showing the expression levels of *FOXD3-AS1*, *PARP1*, *CTCF*, and downstream genes at the endpoints of xenografts in athymic nude mice treated by intratumoral injection of mock, *FOXD3-AS1*, si-Scb, si-PARP1, or si-CTCF, respectively (mean ± SD, n = 5). Analysis of variance and Student's t test were used to analyze differences in (A)–(C) and (E). Log-rank test for survival comparison was used in (D). *p < 0.01 versus mock or si-Scb. NS, not significant.

calculated. Sequencing data have been deposited in the GEO (GEO: GSE105016).

Real-Time qRT-PCR

Nuclear and cytoplasmic RNA was isolated using RNA Subcellular Isolation Kit (Active Motif, Carlsbad, CA). Total RNA was isolated with RNeasy Mini Kit (QIAGEN). Reverse transcription reactions were conducted with the Transcriptor First Strand cDNA Synthesis Kit (Roche). Real-time PCR was performed with SYBR green PCR Master Mix (Applied Biosystems, Foster City, CA) and the primers indicated in Table S7. The transcript levels were analyzed by the $2^{-\Delta\Delta Ct}$ method.

Western Blot

Tissue or cellular protein was extracted with 1 × cell lysis buffer (Promega). Western blot was performed as previously

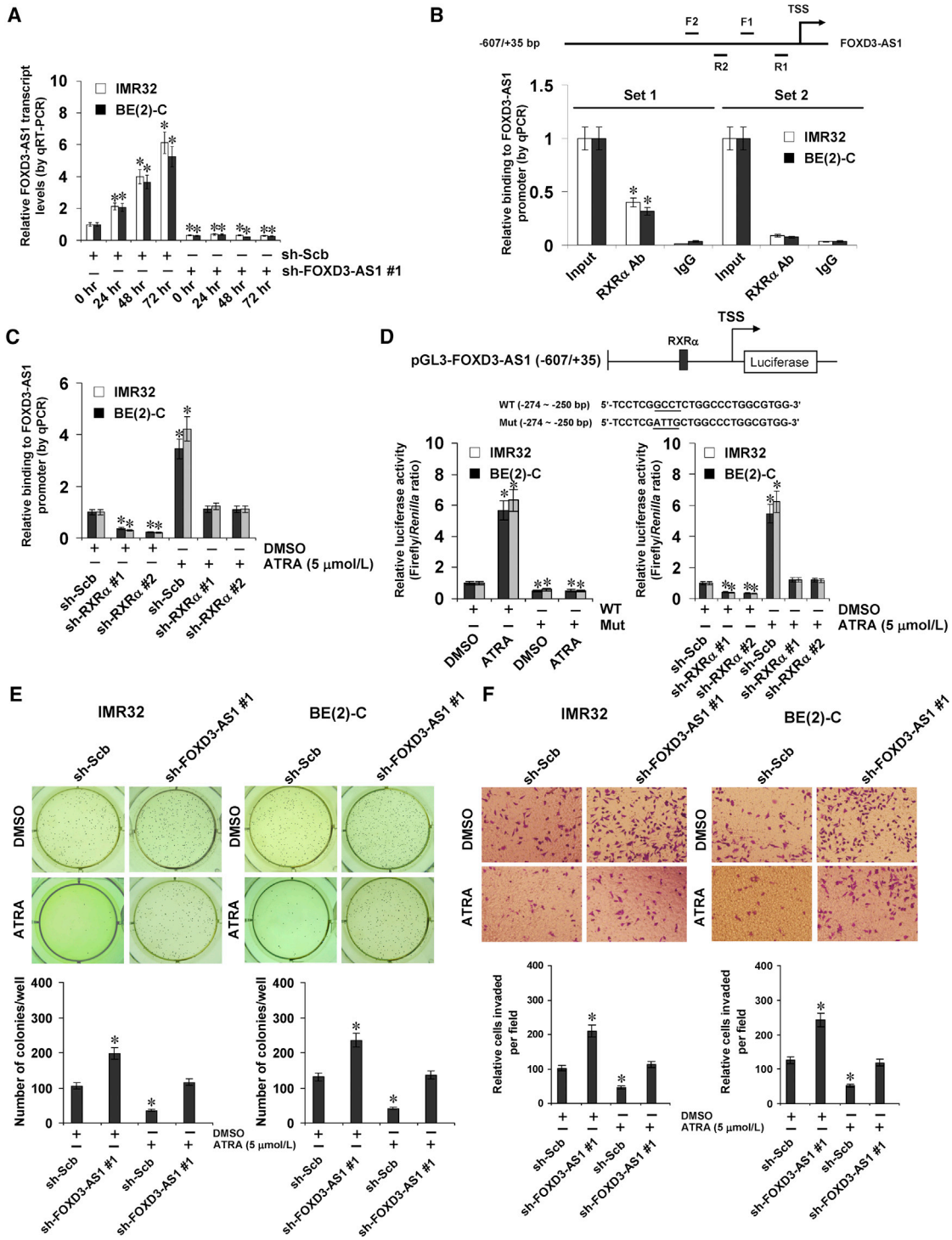

Figure 8. Inducible FOXD3-AS1 Plays Crucial Roles in Retinoic-Acid-Facilitated Differentiation and Tumor Suppression in NB Cells

(A) Real-time qRT-PCR assay indicating the expression of FOXD3-AS1 (normalized to GAPDH) in IMR32 and BE(2)-C cells stably transfected with scramble shRNA (sh-Scb) or sh-FOXD3-AS1 #1 and those treated with ATRA (5 μmol/L) for 24, 48, or 72 hr (mean ± SD, n = 6). (B) ChIP and qPCR assay with two primer sets indicating the endogenous binding of RXRα to *FOXD3-AS1* promoter (normalized to input DNA) in cultured IMR32 and BE(2)-C cells (mean ± SD, n = 5). (C) ChIP and qPCR assay indicating the enrichment of RXRα on *FOXD3-AS1* promoter (normalized to input DNA) in NB cells treated with ATRA (5 μmol/L) for 48 hr and those stably transfected with sh-Scb or sh-RXRα (mean ± SD, n = 5). (D) Dual-luciferase assay showing the activity of *FOXD3-AS1* promoter reporter (normalized to pGL3-Basic) with wild-type (WT) or mutant (Mut)

(legend continued on next page)

described,[7,45–47] with antibodies specific for CTCF (ab188408), FLAG (ab45766), Myc (ab9106), FOXD3 (ab67758), IFIT2 (ab113112), IL6ST (ab202850), KLF6 (ab135783), SAMD9 (ab180575), RXRα (ab24363; Abcam, Cambridge, MA), PARylation (PAR, ALX-804-220; Alexis, San Diego, CA), PAPR1 (sc-1562), GST (sc-33614), H3 histone (sc-10809), and GAPDH (sc-47724; Santa Cruz Biotechnology, Santa Cruz, CA).

Co-IP Assay

The co-IP assay was performed as previously described,[48] with antibodies specific for PAPR1 (sc-1562, Santa Cruz Biotechnology), CTCF (ab188408), FLAG (ab45766), Myc (ab9106, Abcam), or PAR (ALX-804-220, Alexis). Bead-bound protein was released by boiling the protein A-Sepharose beads (Santa Cruz Biotechnology) in 1 × SDS-PAGE loading buffer and analyzed by western blot.

BiFC Assay

Human *PARP1* cDNA (3,045 bp) and *CTCF* cDNA (2,184 bp) were subcloned into the BiFC vectors pBiFC-VN173 and pBiFC-VC155 (Addgene), respectively. Recombinant constructs were co-transfected into tumor cells with Lipofectamine 2000 (Invitrogen) for 24 hr. Cells were then cultured at 37°C for 10 hr to allow maturation of fluorophore. Fluorescence emission was observed under a confocal microscope using excitation and emission wavelengths of 488 and 500 nm, respectively.[49]

Fluorescence Immunocytochemical Staining

Tumor cells were plated on coverslips, fixed with a solution of 95% ethanol and 5% glacial acetic acid, permeabilized with 0.3% Triton X-100, and blocked with 5% milk for 1 hr. Cells were incubated at 4°C overnight with antibodies specific for PARP1 (sc-1562, Santa Cruz Biotechnology; 1:100 dilution), CTCF (ab188408, Abcam; 1:100 dilution), GAP43 (ab12274, Abcam; 1:200 dilution), or NF-200 (MAB5256A5, Millipore; 1:100 dilution). Cells were then incubated with Alexa Fluor 594 goat anti-rabbit immunoglobulin G (IgG; 1:1,000 dilution), stained with DAPI (300 nmol/L) to visualize nuclei, and photographed with a Nikon Eclipse E800 microscope.[7]

Luciferase Reporter Assay

The human *FOXD3* promoter (−1,870/+130), the *FOXD3-AS1* promoter (−607/+35), and its truncates were amplified from genomic DNA by PCR (Table S8) and subcloned into pGL3-Basic (Promega). Mutation of the CTCF- or RXRα-binding site was performed with the GeneTailor Site-Directed Mutagenesis System (Invitrogen) and PCR primers (Table S8). The dual-luciferase assay was performed according to the manufacturer's instructions (Promega, Madison, WI). Luciferase activity was measured with a luminometer (Lumat LB9507, Berthold Tech, Bad Wildbad, Germany).[7,32,48,50–52]

Rescue of Target Gene Expression

To restore the target gene expression induced by *PARP1* or *CTCF* overexpression, tumor cells were transfected with *FOXD3-AS1* expression vector. To rescue gene expression altered by knockdown of *PARP1* or *CTCF*, shRNA specific for *FOXD3-AS1* (Table S9) was transfected into tumor cells with Genesilencer Transfection Reagent (Genlantis, San Diego, CA). Empty vector and sh-Scb were applied as controls (Table S9).

Biotin-Labeled RNA Pull-Down and Mass Spectrometry Analysis

Biotin-labeled RNA probes for *FOXD3-AS1* truncates were *in vitro* transcribed as described above. Biotin-labeled RNA pull-down was performed as previously described.[7] Briefly, cellular nuclear protein was extracted using NE-PER Nuclear and Cytoplasmic Extraction Reagents (Thermo Fisher Scientific) and incubated with biotin-labeled RNAs and streptavidin agarose beads (Invitrogen, Carlsbad, CA). The retrieved protein was detected by western blot or mass spectrometry analysis at Wuhan Institute of Biotechnology (Wuhan, China).

Cross-Linking RIP Assay

Cells were ultraviolet light cross-linked at 254 nm (200 J/cm^2) in PBS and collected by scraping.[7] The RIP assay was performed according to the instructions include with the Magna RIP RNA-Binding Protein Immunoprecipitation Kit (Millipore), with antibodies specific for PARP1 (ab32138 and sc-1562, Abcam and Santa Cruz Biotechnology). Co-precipitated RNAs were detected by RT-PCR with specific primers (Table S7). Total RNA (input) and isotype antibody (IgG) were applied as controls.

In Vitro Binding Assay

A series of *PARP1* truncates were amplified from NB tissues (Table S8), subcloned into pGEX-6P-1 (Addgene), and transformed into *Escherichia coli* to produce GST-tagged truncated PARP1 proteins.[7] *FOXD3-AS1* cRNA was *in vitro* transcribed with the TranscriptAid T7 High Yield Transcription Kit (Thermo Fisher Scientific, Waltham, MA) and incubated with GST-tagged PARP1 protein. PARP1-RNA complexes were pulled down using GST beads (Sigma). Protein was detected by SDS-PAGE and western blot, while RNA was measured by RT-PCR with specific primers (Table S7).

RNA EMSA Assay

The biotin-labeled RNA probe for *FOXD3-AS1* was prepared as described above. RNA EMSA using recombinant PARP1 protein

RXRα-binding site in NB cells treated with ATRA (5 μmol/L) for 48 hr and those stably transfected with sh-Scb or sh-RXRα (mean ± SD, n = 5). (E and F) Representation (top) and quantification (bottom) of soft agar (E) and Matrigel invasion (F) assays indicating the anchorage-independent growth (for 21 days) and invasion (for 24 hr) capability of NB cells stably transfected with sh-Scb or sh-FOXD3-AS1 #1 and those treated with ATRA (5 μmol/L) for 48 hr. Student's t test was used to analyze differences in (A)–(F). *$p < 0.01$ versus sh-Scb at 0 hr, IgG, sh-Scb + DMSO, or WT + DMSO.

was performed according to the instructions included with the LightShift Chemiluminescent RNA EMSA Kit (Thermo Fisher Scientific).

ChIP Assay

The ChIP assay was performed according to the manufacturer's instructions (EZ-ChIP kit; Upstate Biotechnology, Temecula, CA).[32,48,53] Real-time qPCR was performed with SYBR green PCR Master Mix (Applied Biosystems), primers targeting gene promoters (Table S7), and ABI Prism 7700 Sequence Detector (Applied Biosystems). The amount of immunoprecipitated DNA was calculated in reference to a standard curve and normalized to input DNA.

Cellular Viability Assay

Cell viability was monitored by 2-(4,5-dimethyltriazol-2-yl)-2,5-diphenyl tetrazolium bromide (MTT; Sigma) colorimetric assay.[48,51,54] Briefly, 20 μL of MTT (5 mg/ml) was added to each well. After 4 hr of incubation at 37°C, cell supernatants were discarded. MTT crystals were dissolved with DMSO, while absorbance was measured at 570 nm. All experiments were done with 6–8 wells per experiment and repeated at least three times.

Cellular Apoptosis Assay

Apoptosis ratios of cells were determined by Annexin V/FITC and PI staining flow cytometry.[55] Briefly, tumor cells were collected, washed twice with cold PBS, resuspended with 100 μL binding buffer into 2–5 $\times$ 10^5 cells/mL density, and incubated with Annexin V/FITC (BD Pharmingen, San Diego, CA) at room temperature for 10 min. After washing with binding buffer, cells were resuspended with 400 μL binding buffer containing 10 μL PI (20 μg/mL) and incubated on ice for 15 min. Apoptosis was analyzed by a flow cytometer (Becton Dickson) at a wavelength of 488 nm.

Soft Agar Assay

Tumor cells (5 $\times$ 10^3) were mixed with 0.05% Nobel agar (Fisher Scientific, Pittsburgh, PA) in growth medium and plated onto 6-well plates containing a solidified bottom layer (0.1% Noble agar in growth medium). After incubation of cells for 21 days, cells were fixed with 100% methanol and stained with 0.5% crystal violet dye. The number of cell colonies was counted under a microscope.[7,32,45]

Cell Invasion Assay

The Matrigel invasion assay was performed using membranes coated with Matrigel matrix (BD Science, Sparks, MD). Homogeneous single-cell suspensions (1 $\times$ 10^5 cells/well) were added to the top chambers and allowed to invade for 24 hr at 37°C in a CO_2 incubator. Invaded cells were stained with 0.1% crystal violet for 10 min at room temperature and examined by light microscopy. Quantification of invaded cells was performed according to published criteria.[7,45–47,53,56,57]

In Vivo Growth, Metastasis, and Therapeutic Assays

All animal experiments were carried out in accordance with NIH Guidelines for the Care and Use of Laboratory Animals and approved by the Animal Care Committee of Tongji Medical College (approval Y20080290). For *in vivo* tumor growth studies, blindly randomized 4-week-old male BALB/c nude mice (n = 5 per group) were injected subcutaneously in the dorsal flanks with 1 $\times$ 10^6 tumor cells. One month later, mice were sacrificed and examined for tumor weight. Experimental metastasis studies were performed by tail vein injection of tumor cells (0.4 $\times$ 10^6 per mouse, n = 5 per group) into blindly randomized 4-week-old male BALB/c nude mice as previously described.[7,32,45,56] Mice were sacrificed when they became ill or paralyzed. For *in vivo* therapeutic studies, tumor cells (1 $\times$ 10^6) were injected subcutaneously into the dorsal flanks of nude mice. Two weeks after tumor cell inoculation with confirmation of successful maturation of tumors, mice were blindly randomized and treated by intratumoral injection of *FOXD3-AS1* construct or 21-nucleotide synthesized siRNAs (Table S9; RiboBio) using Invivofectamine 3.0 Reagent (Life Technologies) as indicated. Tumor volume, body weight, and survival time of each mouse were monitored and recorded.

Patient Tissue Samples

The institutional review board of Tongji Medical College approved the human tissue study (approval 2011-S085). All procedures were carried out in accordance with approved guidelines. Informed consent was obtained from all patients. Human embryonic tissues or normal dorsal root ganglia were obtained from therapeutic abortions (at day 50 of gestation) and interrupted pregnancies, respectively. Fresh tumor specimens were collected at surgery and stored at −80°C until use. Total RNA of normal human dorsal ganglia was obtained from Clontech.

Immunohistochemistry

Immunohistochemical staining was performed as previously described[7,32,45,56] with an antibody specific for Ki-67 (ab92742, Abcam; 1:100 dilution). The reactivity degree was assessed by at least two pathologists without knowledge of tumor clinicopathological features. The degree of positivity was initially classified according to the percentage of positive tumor cells as follows: −, <5%; 1+, 6%–25%; 2+, 26%–50%; and 3+, >50%. Slides with moderate positive (2+) or strong positive (3+) reactivity were classified as having high expression, whereas slides with negative (−) or weak positive (1+) reactivity were classified as having low expression.

Data Availability

RNA-sequencing data that support the findings of this study have been deposited in the GEO database with the accession code GEO: GSE105016. All remaining data are either contained within this article and Supplemental Information or available from the author on request.

Statistical Analysis

All data are shown as mean ± SD. Cutoff values were determined by average gene expression levels. Student's t test, analysis of variance, χ^2 analysis, and Fisher exact probability analysis were applied to compare differences in tumor cells or tissues. Fisher's exact test was

applied to analyze the statistical significance of overlap between two gene lists. Pearson's correlation coefficient was applied for analyzing the expression correlation of two genes. Log-rank test and Cox regression models were used to assess survival difference and HRs. All statistical tests were two sided.

SUPPLEMENTAL INFORMATION

Supplemental Information includes ten figures and nine tables and can be found with this article online at https://doi.org/10.1016/j.ymthe.2017.12.017.

AUTHOR CONTRIBUTIONS

X.Z. and D.L. conceived and performed most of the experiments. D.H., H.S., and H.M. performed some of the *in vitro* studies. E.F and X.W. performed the *in vivo* experiments. X.Z. and D.L. performed the analysis of publicly available clinical tumor datasets. K.H. critically reviewed the manuscript. L.Z. and Q.T. wrote the manuscript.

CONFLICTS OF INTEREST

The authors declare no conflicts of interest.

ACKNOWLEDGMENTS

We are grateful to Dr. Minglu Liang for technical support in the BiFC assay. We thank Dr. Mariajose Navia Miranda (Tongji Medical College, Huazhong University of Science and Technology, China) for her help with editing the manuscript. This work was supported by the National Natural Science Foundation of China (81272779, 81372667, 81472363, 81402301, 81402408, 81572423, 81672500, 81773094, and 81772967), Fundamental Research Funds for the Central Universities (2012QN224, 2013ZHYX003, 01-18-530112, and 01-18-530115), and the Natural Science Foundation of Hubei Province (2014CFA012).

REFERENCES

1. Brodeur, G.M. (2003). Neuroblastoma: biological insights into a clinical enigma. Nat. Rev. Cancer *3*, 203–216.
2. Park, J.R., Eggert, A., and Caron, H. (2010). Neuroblastoma: biology, prognosis, and treatment. Hematol. Oncol. Clin. North Am. *24*, 65–86.
3. Castelnuovo, M., Massone, S., Tasso, R., Fiorino, G., Gatti, M., Robello, M., Gatta, E., Berger, A., Strub, K., Florio, T., et al. (2010). An Alu-like RNA promotes cell differentiation and reduces malignancy of human neuroblastoma cells. FASEB J. *24*, 4033–4046.
4. Pandey, G.K., Mitra, S., Subhash, S., Hertwig, F., Kanduri, M., Mishra, K., Fransson, S., Ganeshram, A., Mondal, T., Bandaru, S., et al. (2014). The risk-associated long noncoding RNA NBAT-1 controls neuroblastoma progression by regulating cell proliferation and neuronal differentiation. Cancer Cell *26*, 722–737.
5. Liu, P.Y., Erriquez, D., Marshall, G.M., Tee, A.E., Polly, P., Wong, M., Liu, B., Bell, J.L., Zhang, X.D., Milazzo, G., et al. (2014). Effects of a novel long noncoding RNA, lncUSMycN, on N-Myc expression and neuroblastoma progression. J. Natl. Cancer Inst. *106*, dju113.
6. Vance, K.W., Sansom, S.N., Lee, S., Chalei, V., Kong, L., Cooper, S.E., Oliver, P.L., and Ponting, C.P. (2014). The long non-coding RNA Paupar regulates the expression of both local and distal genes. EMBO J. *33*, 296–311.
7. Zhao, X., Li, D., Pu, J., Mei, H., Yang, D., Xiang, X., Qu, H., Huang, K., Zheng, L., and Tong, Q. (2016). CTCF cooperates with noncoding RNA MYCNOS to promote neuroblastoma progression through facilitating MYCN expression. Oncogene *35*, 3565–3576.
8. Wang, L., Park, H.J., Dasari, S., Wang, S., Kocher, J.P., and Li, W. (2013). CPAT: Coding-Potential Assessment Tool using an alignment-free logistic regression model. Nucleic Acids Res. *41*, e74.
9. Michel, A.M., Fox, G., M Kiran, A., De Bo, C., O'Connor, P.B., Heaphy, S.M., Mullan, J.P., Donohue, C.A., Higgins, D.G., and Baranov, P.V. (2014). GWIPS-viz: development of a ribo-seq genome browser. Nucleic Acids Res. *42*, D859–D864.
10. Magan, N., Isaacs, R.J., and Stowell, K.M. (2012). Treatment with the PARP-inhibitor PJ34 causes enhanced doxorubicin-mediated cell death in HeLa cells. Anticancer Drugs *23*, 627–637.
11. Lachmann, A., Xu, H., Krishnan, J., Berger, S.I., Mazloom, A.R., and Ma'ayan, A. (2010). ChEA: transcription factor regulation inferred from integrating genome-wide ChIP-X experiments. Bioinformatics *26*, 2438–2444.
12. Farrar, D., Rai, S., Chernukhin, I., Jagodic, M., Ito, Y., Yammine, S., Ohlsson, R., Murrell, A., and Klenova, E. (2010). Mutational analysis of the poly(ADP-ribosyl)ation sites of the transcription factor CTCF provides an insight into the mechanism of its regulation by poly(ADP-ribosyl)ation. Mol. Cell. Biol. *30*, 1199–1216.
13. Ray Chaudhuri, A., and Nussenzweig, A. (2017). The multifaceted roles of PARP1 in DNA repair and chromatin remodelling. Nat. Rev. Mol. Cell Biol. *18*, 610–621.
14. Han, D., Chen, Q., Shi, J., Zhang, F., and Yu, X. (2017). CTCF participates in DNA damage response via poly(ADP-ribosyl)ation. Sci. Rep. *7*, 43530.
15. Chen, Z.H., Hu, H.K., Zhang, C.R., Lu, C.Y., Bao, Y., Cai, Z., Zou, Y.X., Hu, G.H., and Jiang, L. (2016). Down-regulation of long non-coding RNA FOXD3 antisense RNA 1 (FOXD3-AS1) inhibits cell proliferation, migration, and invasion in malignant glioma cells. Am. J. Transl. Res. *8*, 4106–4119.
16. Zhang, D., Lee, H., Haspel, J.A., and Jin, Y. (2017). Long noncoding RNA FOXD3-AS1 regulates oxidative stress-induced apoptosis via sponging microRNA-150. FASEB J. *31*, 4472–4481.
17. D'Amours, D., Desnoyers, S., D'Silva, I., and Poirier, G.G. (1999). Poly(ADP-ribosyl)ation reactions in the regulation of nuclear functions. Biochem. J. *342*, 249–268.
18. Hassa, P.O., and Hottiger, M.O. (2002). The functional role of poly(ADP-ribose)polymerase 1 as novel coactivator of NF-kappaB in inflammatory disorders. Cell. Mol. Life Sci. *59*, 1534–1553.
19. Simbulan-Rosenthal, C.M., Rosenthal, D.S., Luo, R., Samara, R., Espinoza, L.A., Hassa, P.O., Hottiger, M.O., and Smulson, M.E. (2003). PARP-1 binds E2F-1 independently of its DNA binding and catalytic domains, and acts as a novel coactivator of E2F-1-mediated transcription during re-entry of quiescent cells into S phase. Oncogene *22*, 8460–8471.
20. Nusinow, D.A., Hernández-Muñoz, I., Fazzio, T.G., Shah, G.M., Kraus, W.L., and Panning, B. (2007). Poly(ADP-ribose) polymerase 1 is inhibited by a histone H2A variant, MacroH2A, and contributes to silencing of the inactive X chromosome. J. Biol. Chem. *282*, 12851–12859.
21. Lee, M.H., Na, H., Kim, E.J., Lee, H.W., and Lee, M.O. (2012). Poly(ADP-ribosyl)ation of p53 induces gene-specific transcriptional repression of MTA1. Oncogene *31*, 5099–5107.
22. Rodríguez, M.I., González-Flores, A., Dantzer, F., Collard, J., de Herreros, A.G., and Oliver, F.J. (2011). Poly(ADP-ribose)-dependent regulation of Snail1 protein stability. Oncogene *30*, 4365–4372.
23. Lönn, P., van der Heide, L.P., Dahl, M., Hellman, U., Heldin, C.H., and Moustakas, A. (2010). PARP-1 attenuates Smad-mediated transcription. Mol. Cell *40*, 521–532.
24. Luo, H., Sun, Y., Wei, G., Luo, J., Yang, X., Liu, W., Guo, M., and Chen, R. (2015). Functional characterization of long noncoding RNA Lnc_bc060912 in human lung carcinoma cells. Biochemistry *54*, 2895–2902.
25. Yu, S., Wang, X., Geng, P., Tang, X., Xiang, L., Lu, X., Li, J., Ruan, Z., Chen, J., Xie, G., et al. (2017). Melatonin regulates PARP1 to control the senescence-associated secretory phenotype (SASP) in human fetal lung fibroblast cells. J. Pineal Res. *63*, e12405.
26. Phillips, J.E., and Corces, V.G. (2009). CTCF: master weaver of the genome. Cell *137*, 1194–1211.
27. Filippova, G.N. (2008). Genetics and epigenetics of the multifunctional protein CTCF. Curr. Top. Dev. Biol. *80*, 337–360.
28. Xu, M., Zhao, G.N., Lv, X., Liu, G., Wang, L.Y., Hao, D.L., Wang, J., Liu, D.P., and Liang, C.C. (2014). CTCF controls HOXA cluster silencing and mediates

PRC2-repressive higher-order chromatin structure in NT2/D1 cells. Mol. Cell. Biol. *34*, 3867–3879.

29. Klenova, E.M., Morse, H.C., 3rd, Ohlsson, R., and Lobanenkov, V.V. (2002). The novel BORIS + CTCF gene family is uniquely involved in the epigenetics of normal biology and cancer. Semin. Cancer Biol. *12*, 399–414.
30. Docquier, F., Farrar, D., D'Arcy, V., Chernukhin, I., Robinson, A.F., Loukinov, D., Vatolin, S., Pack, S., Mackay, A., Harris, R.A., et al. (2005). Heightened expression of CTCF in breast cancer cells is associated with resistance to apoptosis. Cancer Res. *65*, 5112–5122.
31. Fiorentino, F.P., Macaluso, M., Miranda, F., Montanari, M., Russo, A., Bagella, L., and Giordano, A. (2011). CTCF and BORIS regulate Rb2/p130 gene transcription: a novel mechanism and a new paradigm for understanding the biology of lung cancer. Mol. Cancer Res. *9*, 225–233.
32. Li, D., Mei, H., Qi, M., Yang, D., Zhao, X., Xiang, X., Pu, J., Huang, K., Zheng, L., and Tong, Q. (2013). FOXD3 is a novel tumor suppressor that affects growth, invasion, metastasis and angiogenesis of neuroblastoma. Oncotarget *4*, 2021–2044.
33. Hromas, R., Ye, H., Spinella, M., Dmitrovsky, E., Xu, D., and Costa, R.H. (1999). Genesis, a Winged Helix transcriptional repressor, has embryonic expression limited to the neural crest, and stimulates proliferation in vitro in a neural development model. Cell Tissue Res. *297*, 371–382.
34. Lai, K.C., Liu, C.J., Chang, K.W., and Lee, T.C. (2013). Depleting IFIT2 mediates atypical PKC signaling to enhance the migration and metastatic activity of oral squamous cell carcinoma cells. Oncogene *32*, 3686–3697.
35. Taniguchi, K., Moroishi, T., de Jong, P.R., Krawczyk, M., Grebbin, B.M., Luo, H., Xu, R.H., Golob-Schwarzl, N., Schweiger, C., Wang, K., et al. (2017). YAP-IL-6ST autoregulatory loop activated on APC loss controls colonic tumorigenesis. Proc. Natl. Acad. Sci. USA *114*, 1643–1648.
36. Gao, Y., Li, H., Ma, X., Fan, Y., Ni, D., Zhang, Y., Huang, Q., Liu, K., Li, X., Wang, L., et al. (2017). KLF6 suppresses metastasis of clear cell renal cell carcinoma via transcriptional repression of E2F1. Cancer Res. *77*, 330–342.
37. Ma, Q., Yu, T., Ren, Y.Y., Gong, T., and Zhong, D.S. (2014). Overexpression of SAMD9 suppresses tumorigenesis and progression during non small cell lung cancer. Biochem. Biophys. Res. Commun. *454*, 157–161.
38. Guastafierro, T., Catizone, A., Calabrese, R., Zampieri, M., Martella, O., Bacalini, M.G., Reale, A., Di Girolamo, M., Miccheli, M., Farrar, D., et al. (2013). ADP-ribose polymer depletion leads to nuclear Ctcf re-localization and chromatin rearrangement(1). Biochem. J. *449*, 623–630.
39. Torrano, V., Navascués, J., Docquier, F., Zhang, R., Burke, L.J., Chernukhin, I., Farrar, D., León, J., Berciano, M.T., Renkawitz, R., et al. (2006). Targeting of CTCF to the nucleolus inhibits nucleolar transcription through a poly(ADP-ribosyl)ation-dependent mechanism. J. Cell Sci. *119*, 1746–1759.
40. Janesick, A., Wu, S.C., and Blumberg, B. (2015). Retinoic acid signaling and neuronal differentiation. Cell. Mol. Life Sci. *72*, 1559–1576.
41. Zhao, H., Zhang, X., Frazão, J.B., Condino-Neto, A., and Newburger, P.E. (2013). HOX antisense lincRNA HOXA-AS2 is an apoptosis repressor in all trans retinoic acid treated NB4 promyelocytic leukemia cells. J. Cell. Biochem. *114*, 2375–2383.
42. Zeng, C., Xu, Y., Xu, L., Yu, X., Cheng, J., Yang, L., Chen, S., and Li, Y. (2014). Inhibition of long non-coding RNA NEAT1 impairs myeloid differentiation in acute promyelocytic leukemia cells. BMC Cancer *14*, 693.
43. Gu, C., Tong, Q., Zheng, L., Liang, Z., Pu, J., Mei, H., Hu, T., Du, Z., Tian, F., and Zeng, F. (2010). TSEG-1, a novel member of histone H2A variants, participates in spermatogenesis via promoting apoptosis of spermatogenic cells. Genomics *95*, 278–289.
44. Subramanian, A., Tamayo, P., Mootha, V.K., Mukherjee, S., Ebert, B.L., Gillette, M.A., Paulovich, A., Pomeroy, S.L., Golub, T.R., Lander, E.S., and Mesirov, J.P. (2005). Gene set enrichment analysis: a knowledge-based approach for interpreting genome-wide expression profiles. Proc. Natl. Acad. Sci. USA *102*, 15545–15550.
45. Zhang, H., Pu, J., Qi, T., Qi, M., Yang, C., Li, S., Huang, K., Zheng, L., and Tong, Q. (2014). MicroRNA-145 inhibits the growth, invasion, metastasis and angiogenesis of neuroblastoma cells through targeting hypoxia-inducible factor 2 alpha. Oncogene *33*, 387–397.
46. Zheng, L., Qi, T., Yang, D., Qi, M., Li, D., Xiang, X., Huang, K., and Tong, Q. (2013). microRNA-9 suppresses the proliferation, invasion and metastasis of gastric cancer cells through targeting cyclin D1 and Ets1. PLoS ONE *8*, e55719.
47. Zheng, L., Pu, J., Qi, T., Qi, M., Li, D., Xiang, X., Huang, K., and Tong, Q. (2013). miRNA-145 targets v-ets erythroblastosis virus E26 oncogene homolog 1 to suppress the invasion, metastasis, and angiogenesis of gastric cancer cells. Mol. Cancer Res. *11*, 182–193.
48. Jiang, G., Zheng, L., Pu, J., Mei, H., Zhao, J., Huang, K., Zeng, F., and Tong, Q. (2012). Small RNAs targeting transcription start site induce heparanase silencing through interference with transcription initiation in human cancer cells. PLoS ONE *7*, e31379.
49. Kerppola, T.K. (2008). Bimolecular fluorescence complementation (BiFC) analysis as a probe of protein interactions in living cells. Annu. Rev. Biophys. *37*, 465–487.
50. Li, D., Zhao, X., Xiao, Y., Mei, H., Pu, J., Xiang, X., Jiao, W., Song, H., Qu, H., Huang, K., et al. (2015). Intelectin 1 suppresses tumor progression and is associated with improved survival in gastric cancer. Oncotarget *6*, 16168–16182.
51. Li, D., Mei, H., Pu, J., Xiang, X., Zhao, X., Qu, H., Huang, K., Zheng, L., and Tong, Q. (2015). Intelectin 1 suppresses the growth, invasion and metastasis of neuroblastoma cells through up-regulation of N-myc downstream regulated gene 2. Mol. Cancer *14*, 47.
52. Xiang, X., Zhao, X., Qu, H., Li, D., Yang, D., Pu, J., Mei, H., Zhao, J., Huang, K., Zheng, L., and Tong, Q. (2015). Hepatocyte nuclear factor 4 alpha promotes the invasion, metastasis and angiogenesis of neuroblastoma cells via targeting matrix metalloproteinase 14. Cancer Lett. *359*, 187–197.
53. Zheng, L., Li, D., Xiang, X., Tong, L., Qi, M., Pu, J., Huang, K., and Tong, Q. (2013). Methyl jasmonate abolishes the migration, invasion and angiogenesis of gastric cancer cells through down-regulation of matrix metalloproteinase 14. BMC Cancer *13*, 74.
54. Zheng, L., Jiao, W., Song, H., Qu, H., Li, D., Mei, H., Chen, Y., Yang, F., Li, H., Huang, K., and Tong, Q. (2016). miRNA-558 promotes gastric cancer progression through attenuating Smad4-mediated repression of heparanase expression. Cell Death Dis. *7*, e2382.
55. Tong, Q.S., Jiang, G.S., Zheng, L.D., Tang, S.T., Cai, J.B., Liu, Y., Zeng, F.Q., and Dong, J.H. (2008). Natural jasmonates of different structures suppress the growth of human neuroblastoma cell line SH-SY5Y and its mechanisms. Acta Pharmacol. Sin. *29*, 861–869.
56. Zhang, H., Qi, M., Li, S., Qi, T., Mei, H., Huang, K., Zheng, L., and Tong, Q. (2012). microRNA-9 targets matrix metalloproteinase 14 to inhibit invasion, metastasis, and angiogenesis of neuroblastoma cells. Mol. Cancer Ther. *11*, 1454–1466.
57. Zheng, L., Jiang, G., Mei, H., Pu, J., Dong, J., Hou, X., and Tong, Q. (2010). Small RNA interference-mediated gene silencing of heparanase abolishes the invasion, metastasis and angiogenesis of gastric cancer cells. BMC Cancer *10*, 33.

YMTHE, Volume *26*

Supplemental Information

Risk-Associated Long Noncoding RNA FOXD3-AS1 Inhibits Neuroblastoma Progression by Repressing PARP1-Mediated Activation of CTCF

Xiang Zhao, Dan Li, Dandan Huang, Huajie Song, Hong Mei, Erhu Fang, Xiaojing Wang, Feng Yang, Liduan Zheng, Kai Huang, and Qiangsong Tong

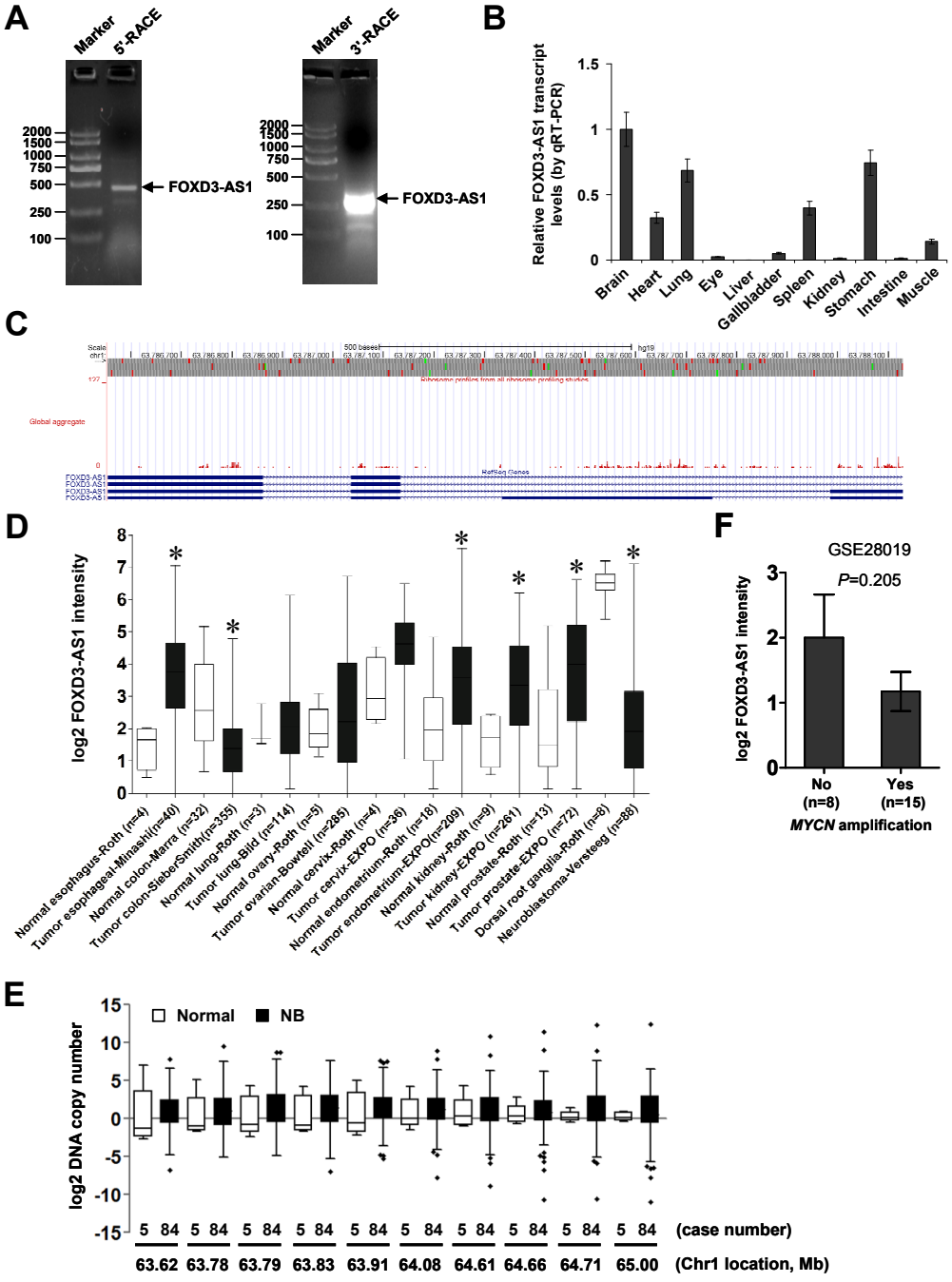

Figure S1 Characterization of a novel lncRNA FOXD3-AS1. (**A**) 5'- and 3'-RACE assays for identifying the full-length sequence of *FOXD3-AS1* in SH-SY5Y cells. (**B**) Real-time qRT-PCR indicating the FOXD3-AS1 levels (normalized to GAPDH) in human embryonic tissues (at day 50 of gestation, mean±SD, n=3). (**C**) Ribosome profiling data showing protein-coding potential of *FOXD3-AS1*. (**D**) Mining of public TCGA datasets indicating the FOXD3-AS1 levels in human tumors and their normal counterparts. (**E**) Representative CGH profile of *FOXD3-AS1* gene locus, locating at chr1:63786555-63788129, in NB tissues derived from Oncogenomics database (https://pob.abcc.ncifcrf.gov/cgi-bin/JK). (**F**) Mining of public dataset (GSE28019) revealing the FOXD3-AS1 levels in NB cell lines with different status of *MYCN* amplification. Student's *t* test analyzed the difference in **D**-**F**. **P*<0.01 vs. normal.

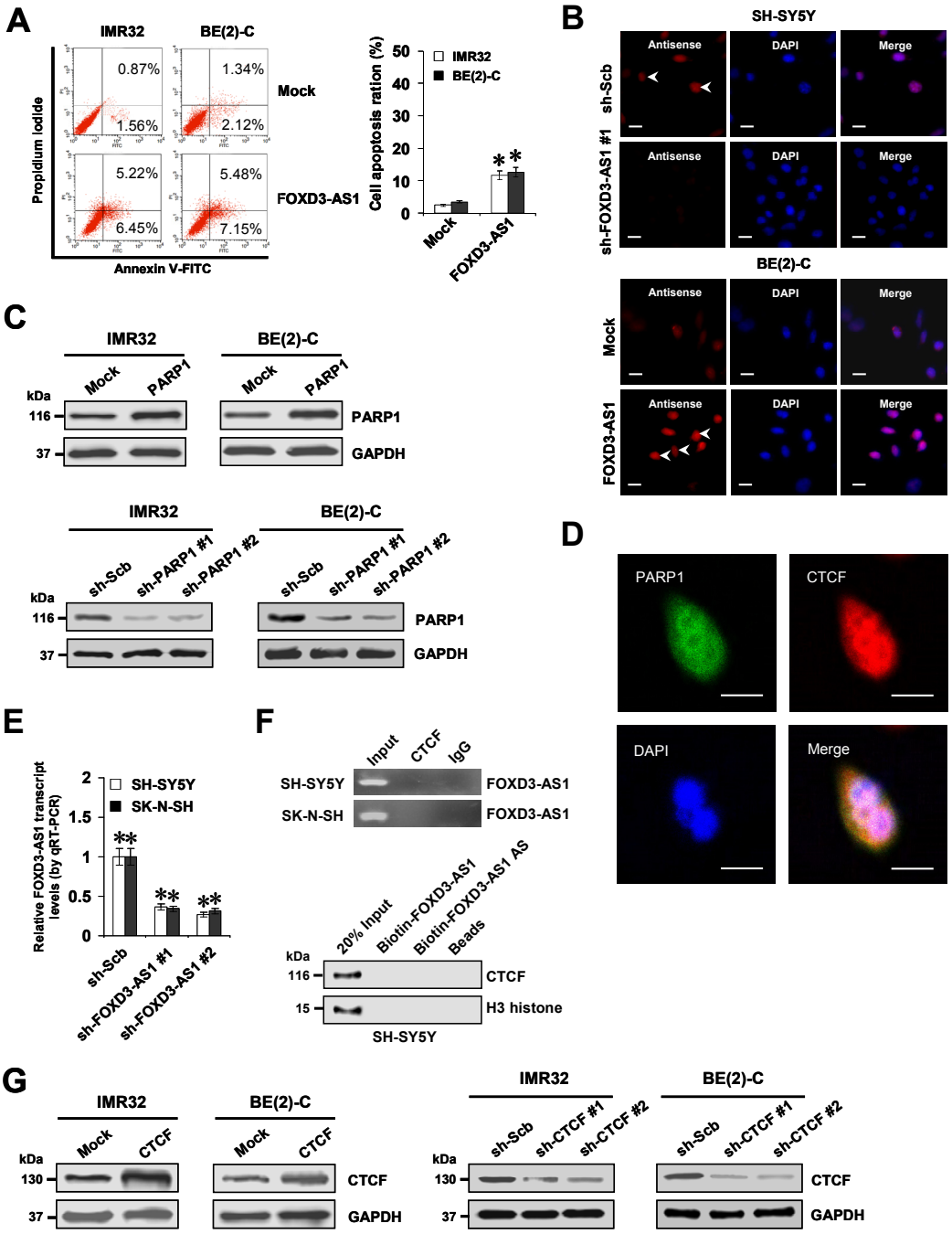

Figure S2 Expression and functions of PARP1, CTCF, and FOXD3-AS1 in NB cells. (**A**) Annexin V-FITC and propidium iodide staining flow cytometry (left panel) and quantification (right panel) depicting the change in apoptosis (after culture for 3 days) of NB cells stably transfected with *FOXD3-AS1*, than those transfected with empty vector (mock; mean ± SD, n=5). (**B**) RNA fluorescence in situ hybridization with a 310-bp antisense probe (red) showing the nuclear localization of FOXD3-AS1 in SH-SY5Y and BE(2)-C cells stably transfected with scramble shRNA (sh-Scb), sh-FOXD3-AS1 #1, empty vector (mock), or FOXD3-AS1. Scale bars: 10 μm. (**C** and **G**) Western blot assay showing the expression levels of PARP1 (C) and CTCF (G) (normalized to GAPDH) in IMR32 and BE(2)-C cells transfected with mock, *PARP1*, *CTCF*, sh-Scb, sh-PARP1, or sh-CTCF for 72 hrs. (**D**) Fluroscence immunocytochemical staining showing the co-localization of PARP1 and CTCF in BE(2)-C cells. Scale bars: 100 μm. (**E**) Real-time qRT-PCR assay indicating the expression of FOXD3-AS1 (normalized to GAPDH) in SH-SY5Y and SK-N-SH cells stably transfected with sh-Scb or sh-FOXD3-AS1 (mean ± SD, n=5). (**F**) RIP (upper panel) and biotin-labeled RNA pull-down (lower panel) assays showing the interaction between FOXD3-AS1 and CTCF in SH-SY5Y cells. Student's *t* test analyzed the difference in **A** and **E**. **P*<0.01 vs. mock or sh-Scb.

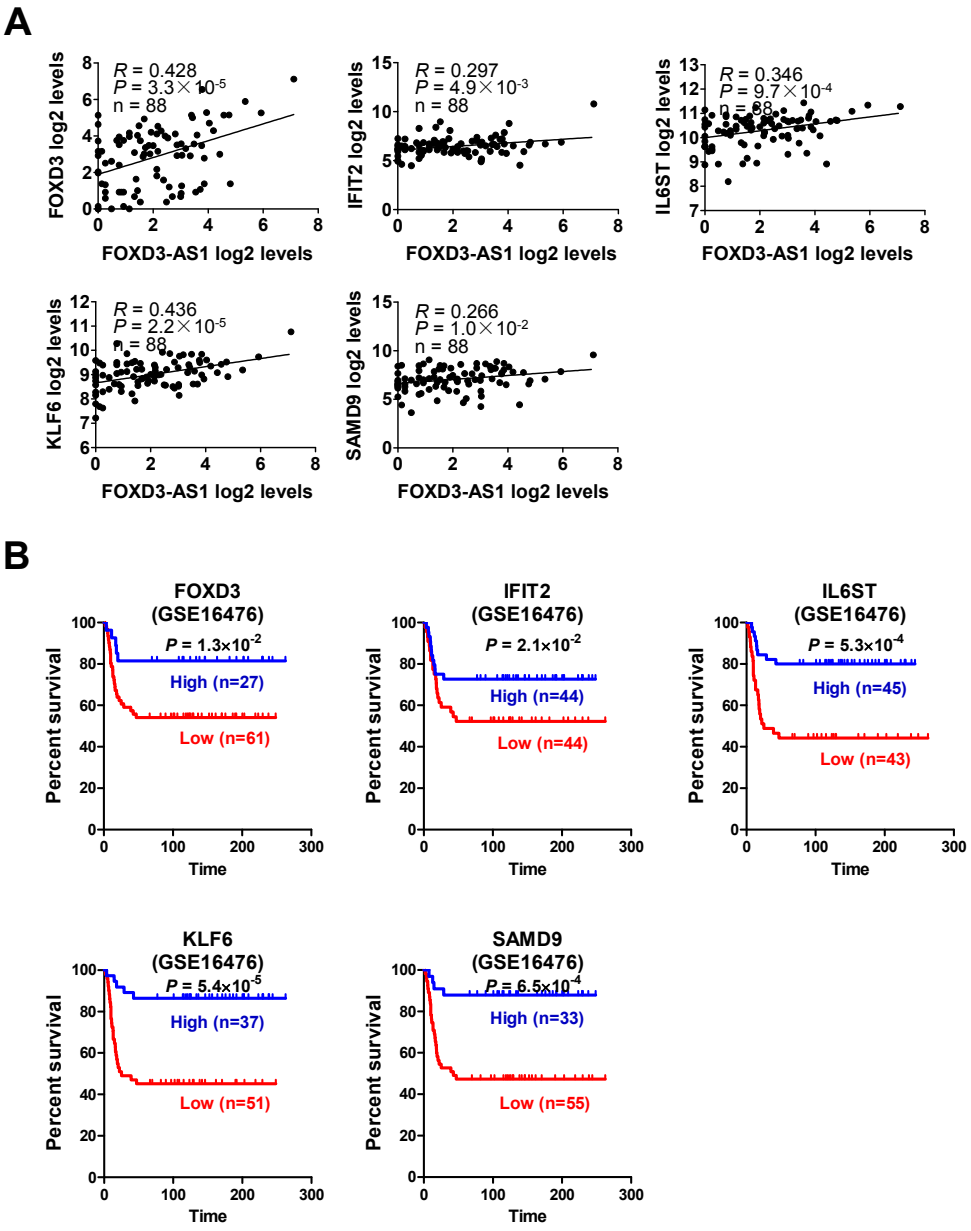

Figure S3 Expression profiles and Kaplan–Meier survival plots of FOXD3-AS1 downstream genes in public datasets. (**A**) The expression correlation between *FOXD3-AS1* and downstream target genes *FOXD3*, *IFIT2*, *IL6ST*, *KLF6*, and *SAMD9* in 88 well-defined NB patients (GSE16476). (**B**) Mining of public dataset (GSE16476) indicating the survival curve of NB patients with high or low levels of *FOXD3* (cutoff value=13.5), *IFIT2* (cutoff value=86.5), *IL6ST* (cutoff value=1357.4), *KLF6* (cutoff value=559.2), and *SAMD9* (cutoff value=175.9). Pearson's correlation coefficient analysis for gene expression in **A**. Log-rank test for survival comparison in **B**.

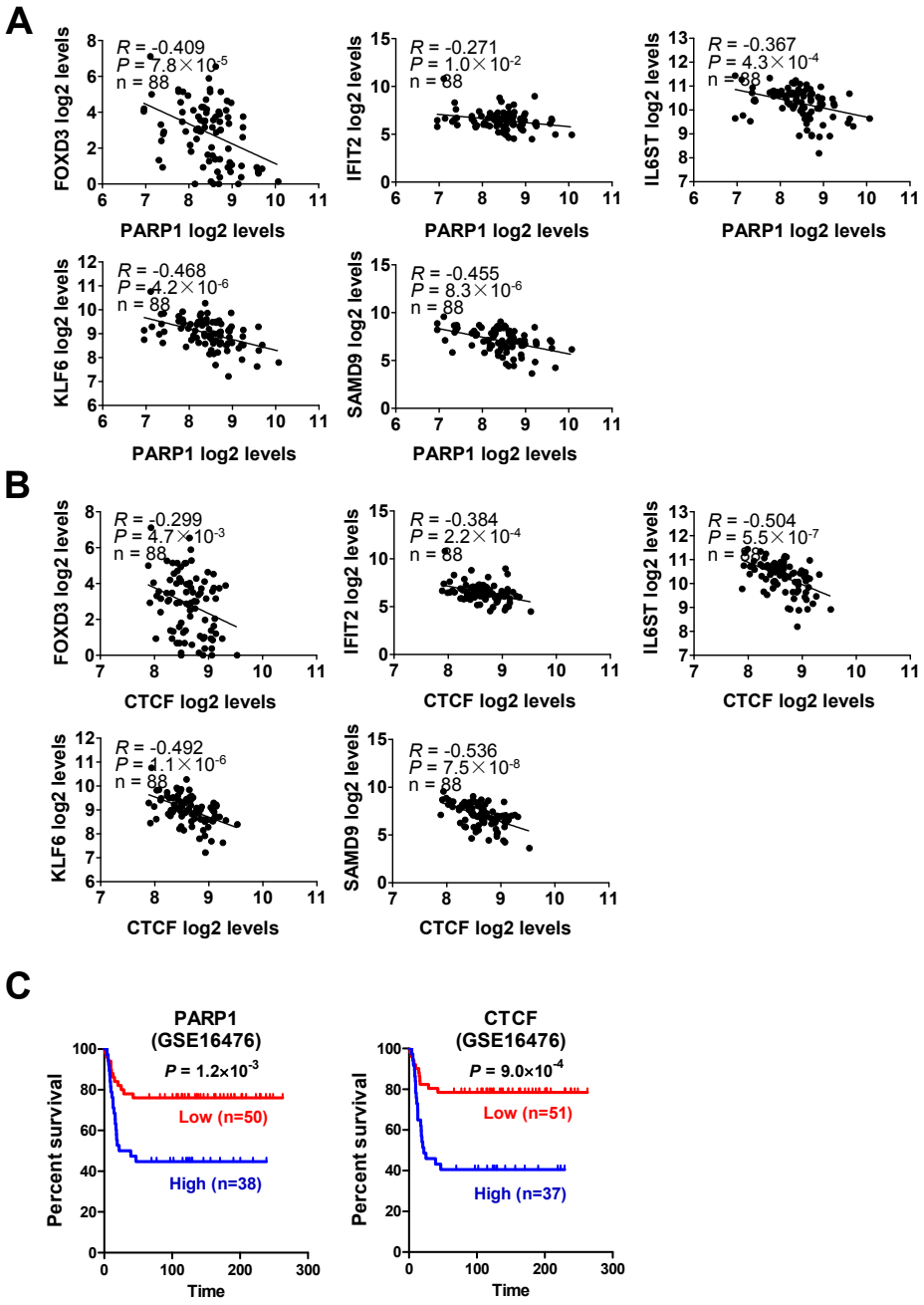

Figure S4 Expression profiles and Kaplan–Meier survival plots of PARP1 and CTCF in public datasets. (**A** and **B**) The expression correlation between *PARP1* (A) or *CTCF* (B) and downstream target genes *FOXD3*, *IFIT2*, *IL6ST*, *KLF6*, and *SAMD9* in 88 well-defined NB patients (GSE16476). (**C**) Mining of public dataset (GSE16476) indicating the survival curves of NB patients with high or low levels of *PARP1* (cutoff value=380.6) and *CTCF* (cutoff value=409.6). Pearson's correlation coefficient analysis for gene expression in **A** and **B**. Log-rank test for survival comparison in **C**.

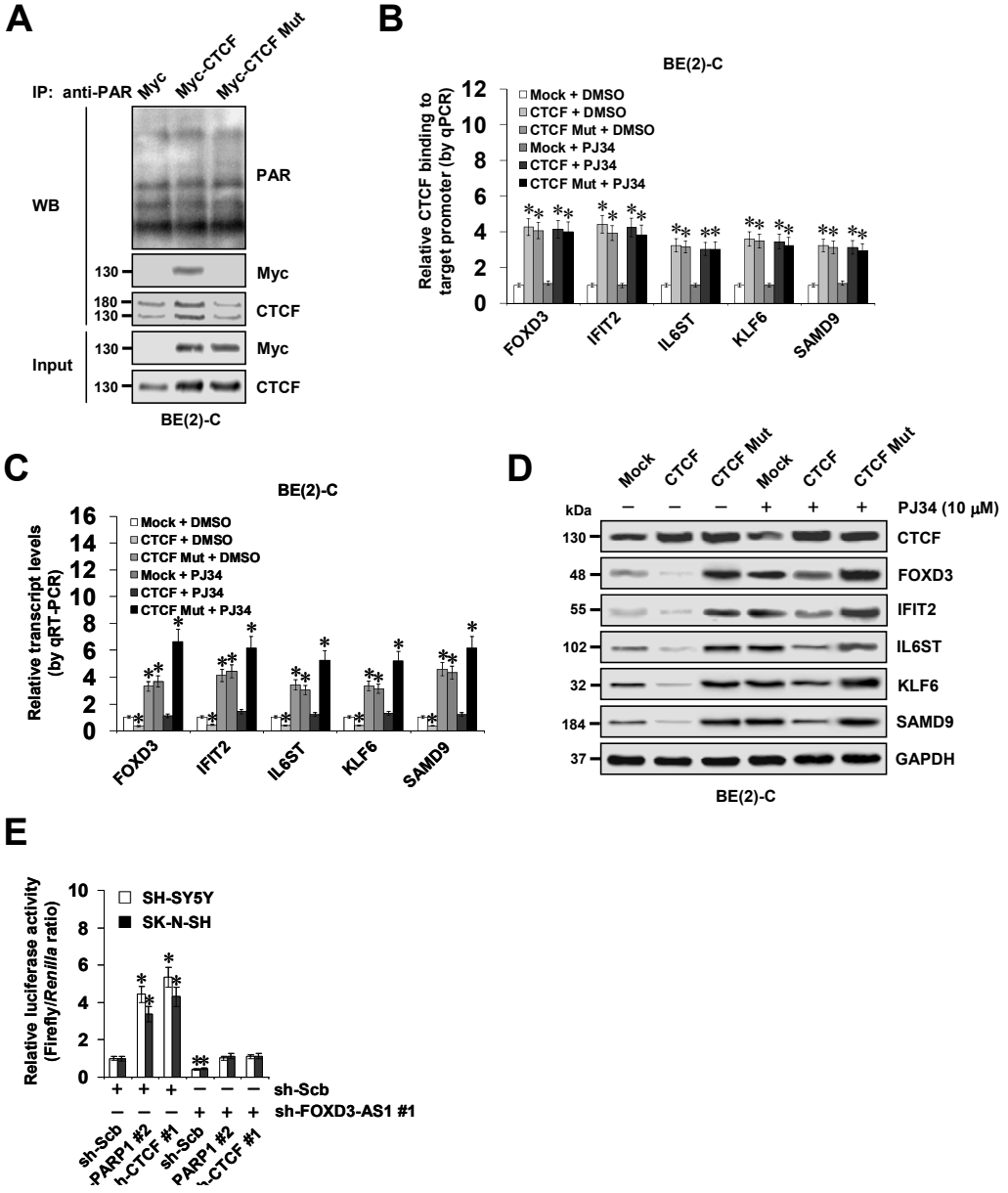

Figure S5 Roles of PARP1-mediated PARylation in regulating CTCF activity. (**A**) IP and western blot assays showing the expression of PARylated CTCF in NB cells transfected with empty vector (mock), wild type *CTCF*, or mutant *CTCF* (*CTCF Mut*) for 72 hrs. (**B**) ChIP and qPCR assay using a CTCF antibody indicating the binding of CTCF to target gene promoters in NB cells transfected with mock, *CTCF*, or *CTCF Mut* for 72 hrs, and those treated with PJ34 (10 μmol/L) for 24 hrs. (**C** and **D**) Real-time qRT-PCR (C) and western blot (D) assays showing the transcript and protein levels of target genes in NB cells transfected with mock, *CTCF*, or *CTCF Mut* for 72 hrs, and those treated with PJ34 (10 μmol/L) for 24 hrs. (**E**) Dual-luciferase assay indicating the relative activity of *FOXD3* promoter (24 hrs post-transfection) in NB cells stably transfected with sh-Scb or sh-FOXD3-AS1 #1, and those co-transfected with sh-PARP1 #2 or sh-CTCF #1 (mean ± SD, n=5). Student's *t* test analyzed the difference in **B**, **C** and **E**. **P*<0.01 vs. mock+DMSO or sh-Scb.

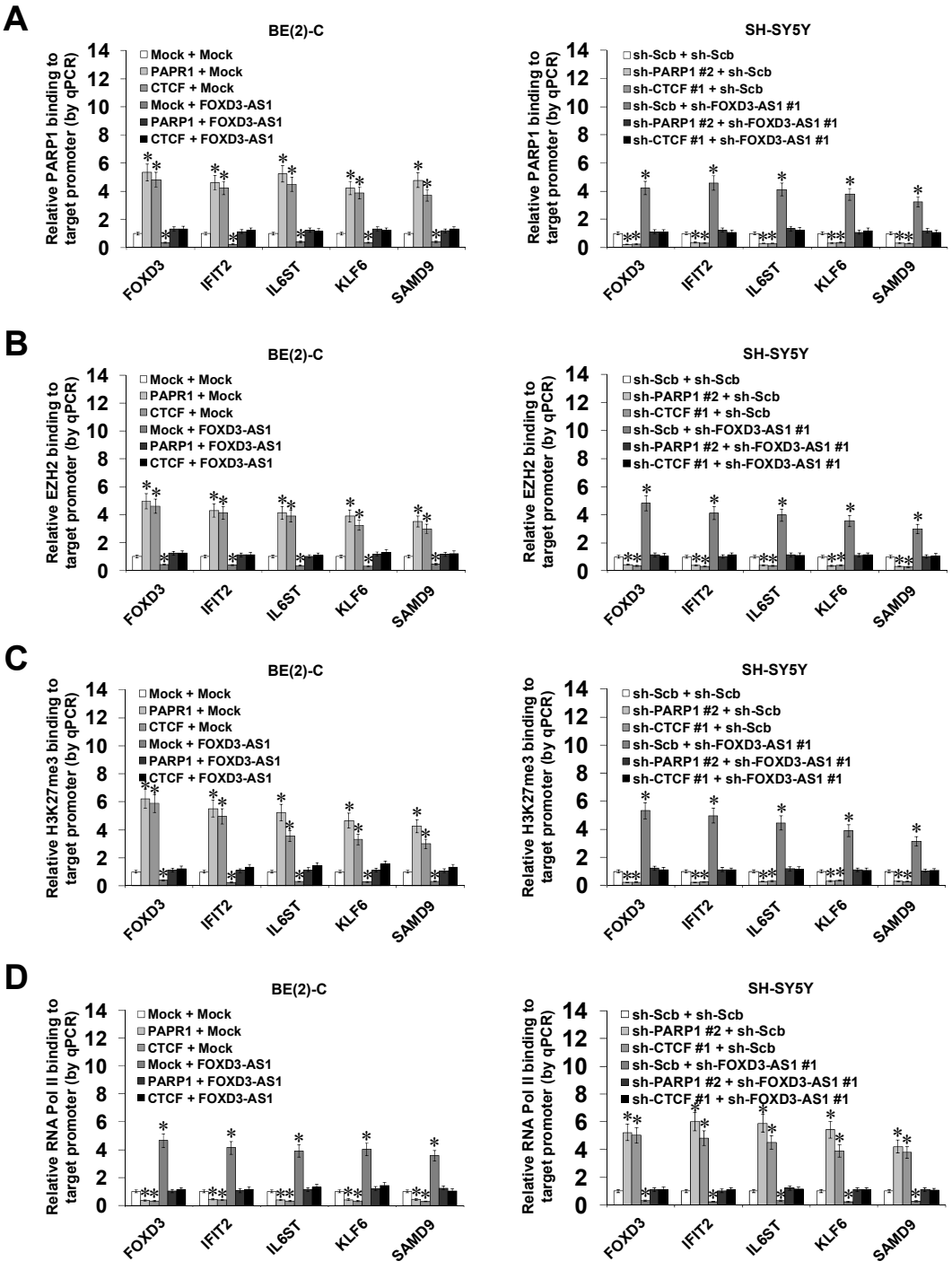

Figure S6 Binding of PARP1, EZH2, H3K27me3, and RNA Pol II to target gene promoters. ChIP and qPCR assay indicating the enrichment of PARP1 (**A**), EZH2 (**B**), H3K27me3 (**C**), and RNA Pol II (**D**) on target gene promoters (normalized to input DNA) in BE(2)-C and SH-SY5Y cells stably transfected with empty vector (mock), *FOXD3-AS1*, scramble shRNA (sh-Scb), or sh-FOXD3-AS1 #1, and those co-transfected with *PARP1*, *CTCF*, sh-PARP1 #2, or sh-CTCF #1 (mean ± SD, n=5). Student's *t* test analyzed the difference in **A**-**D**. **P*<0.01 vs. mock or sh-Scb.

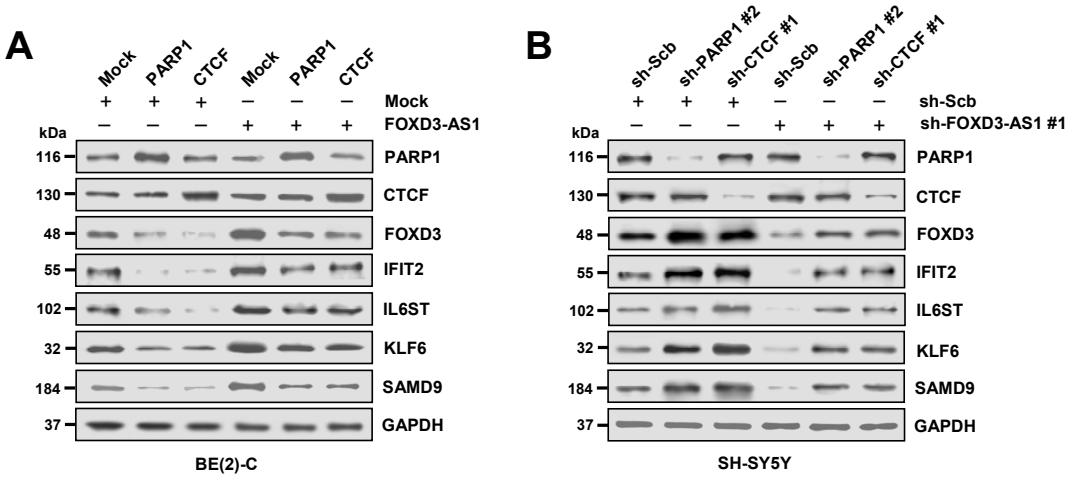

Figure S7 Effects of FOXD3-AS1, PARP1, and CTCF on downstream gene expression in NB cells. (**A** and **B**) Western blot assay showing the expression levels of PARP1, CTCF, and downstream genes *FOXD3*, *IFIT2*, *IL6ST*, *KLF6*, and *SAMD9* (normalized to GAPDH) in NB cells stably transfected with empty vector (mock), *FOXD3-AS1*, scramble shRNA (sh-Scb), or sh-FOXD3-AS1 #1, and those co-transfected with *PARP1*, *CTCF*, sh-PARP1 #2, or sh-CTCF #1.

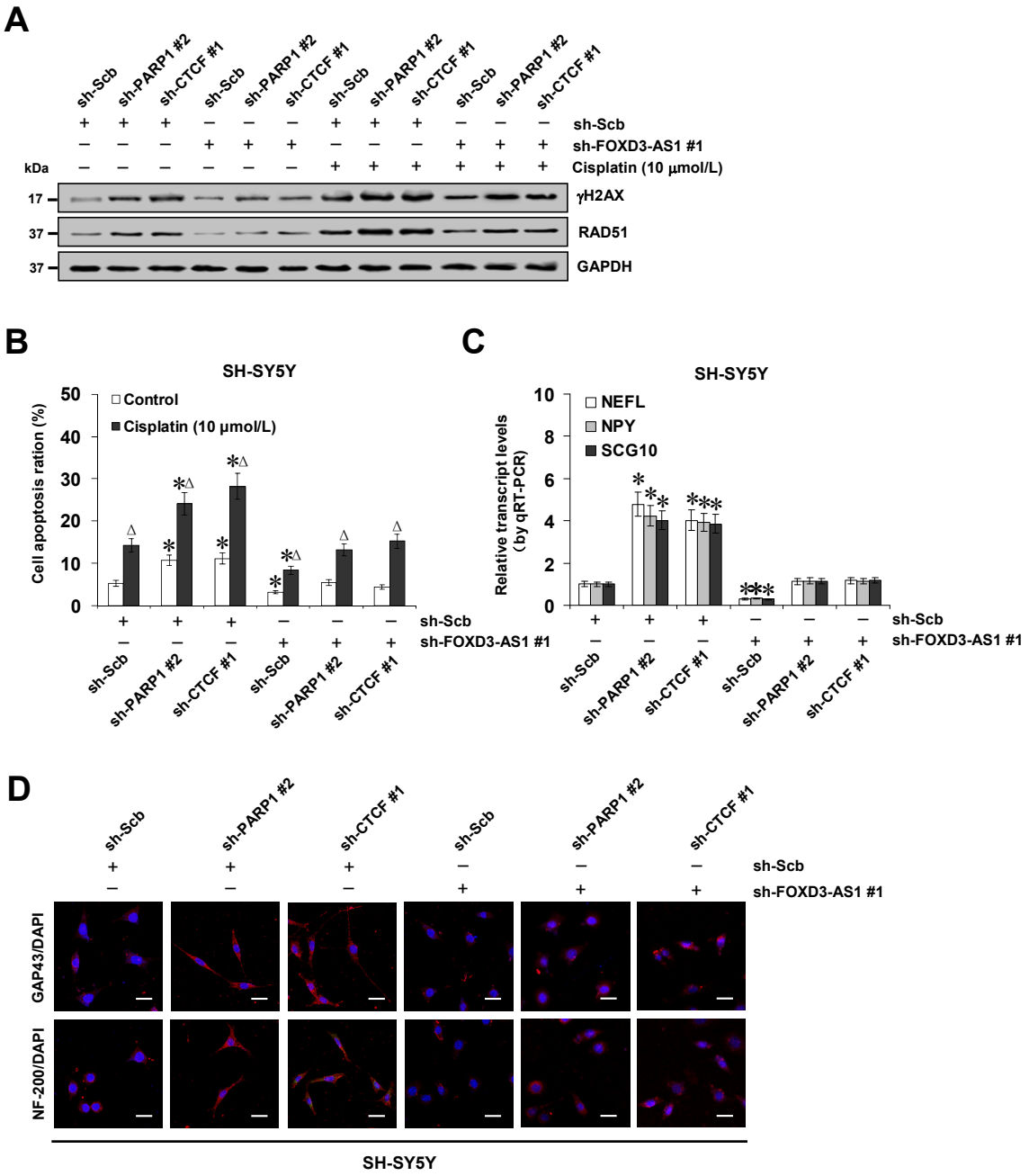

Figure S8 Effects of FOXD3-AS1, PARP1, and CTCF on DNA damage-induced apoptosis and neuronal differentiation of NB cells. (**A** and **B**) Western blot (A) and annexin V-FITC and propidium iodide staining flow cytometry (B) assays indicating the expression of γH2AX and RAD51 and apoptosis in SH-SY5Y cells stably transfected with scramble shRNA (sh-Scb), sh-FOXD3-AS1 #1, sh-PARP1 #2, or sh-CTCF #1, with/without treatment with cisplatin for 24 hrs. (**C**) Real-time qRT-PCR showing the neuronal differentiation marker levels (normalized to GAPDH) in SH-SY5Y cells stably transfected with sh-Scb or sh-FOXD3-AS1 #1, and those co-transfected with sh-PARP1 #2 or sh-CTCF #1. (**D**) Fluroscence immunocytochemical staining assays indicating the neuronal differentiation of NB cells stably transfected with sh-Scb or sh-FOXD3-AS1 #1, and those co-transfected with sh-PARP1 #2 or sh-CTCF #1. Scale bars: 10 μm. Student's *t* test analyzed the difference in **B** and **C**. **P*<0.01 vs. sh-Scb. △ *P*<0.01 vs. control.

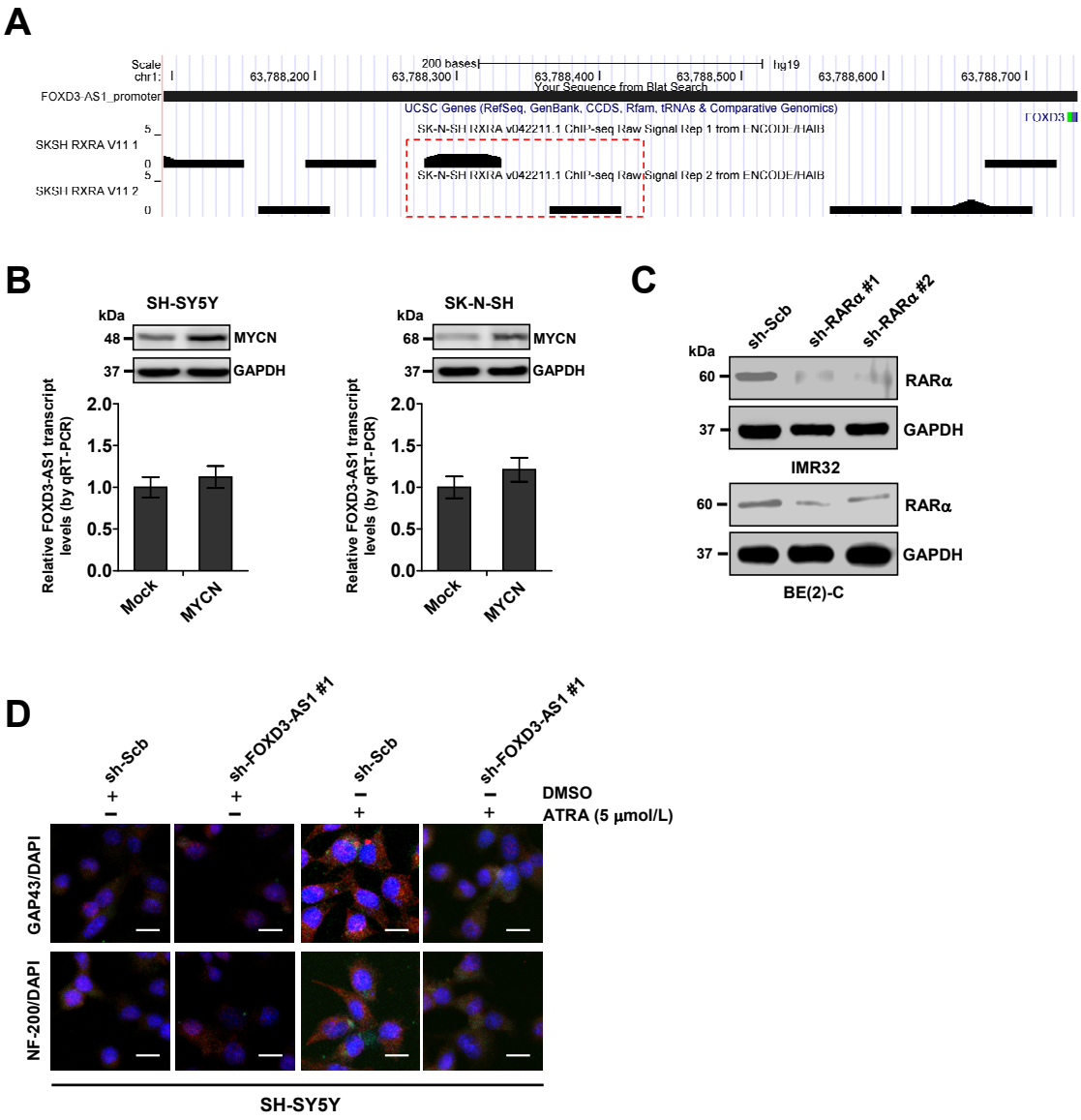

Figure S9 Effects of *RXR α* knockdown and neuronal differentiation of NB cells. (**A**) UCSC Genome Browser view indicating the endogenous binding of RXRα to *FOXD3-AS1* promoter in SK-N-SH cells. (**B**) Real-time qRT-PCR (lower panel) and western blot (upper panel) indicating the FOXD3-AS1 levels (normalized to GAPDH) in NB cells transfected with mock or *MYCN* for 72 hrs (mean ± SD, n=6). (**C**) Western blot assay showing the RXRα expression levels (normalized to GAPDH) in IMR32 and BE(2)-C cells transfected with scramble shRNA (sh-Scb) or sh-RXRα for 48 hrs. (**D**) Fluorescence immunocytochemical staining assays indicating the neuronal differentiation of NB cells stably transfected with sh-Scb or sh-FOXD3-AS1 #1, and those treated with treated with ATRA (5 μmol/L) for 48 hrs.

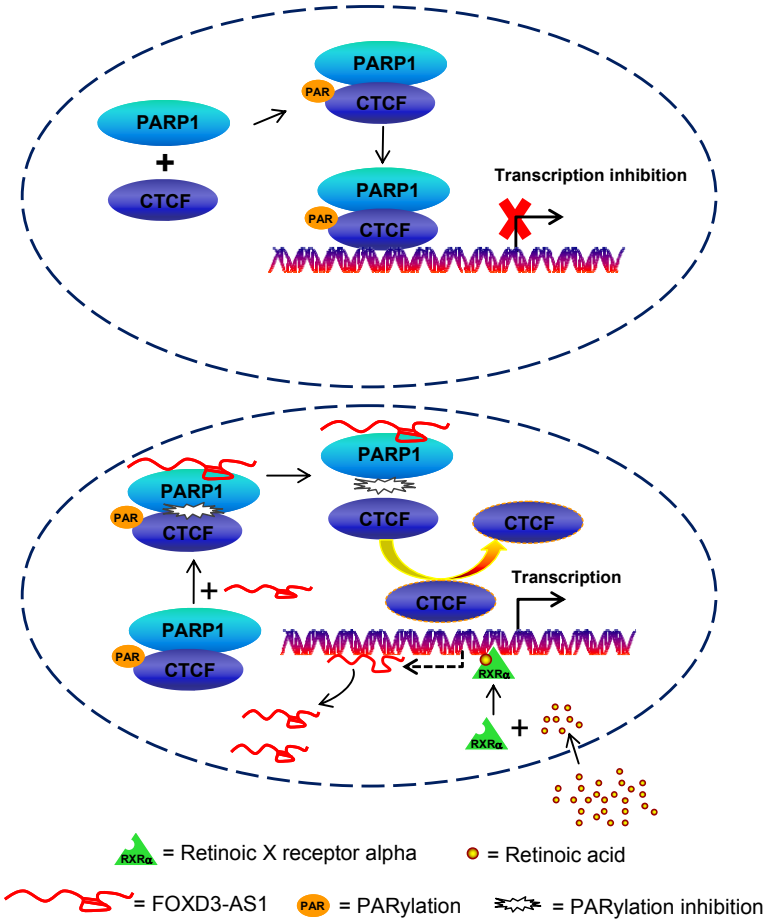

Figure S10 Mechanisms underlying FOXD3-AS1-inhibited progression of NB. As a retinoic acid-inducible lncRNA, FOXD3-AS1 binds to PARP1 protein to repress its physical interaction with CTCF, which in turn decreases the PARylation and activation of CTCF, resulting in derepressed expression of downstream target genes and suppression of NB progression.

Table S1 Log-rank test and Cox regression analyses of lncRNAs crucial for survival of NB patients (GSE16476)

LncRNA symbol	Full name of lncRNA	Log rank test *P*-value	Cox regression *P*-value	Hazard ratio	95% CI
FOXD3-AS1	FOXD3 antisense RNA 1	8.50×10^{-3}	0.004	0.472	0.313-1.446
LINC01268	long intergenic non-protein coding RNA 1268	3.90×10^{-3}	0.387	0.675	0.278-1.642
ZNF667-AS1	ZNF667 antisense RNA 1	1.20×10^{-3}	0.192	2.277	0.661-4.840
FOXCUT	FOXC1 upstream transcript	1.20×10^{-3}	0.006	2.189	1.386-4.334
NBAT1	neuroblastoma associated transcript 1	1.30×10^{-2}	0.139	0.550	0.249-1.215

95% CI, 95% confidence interval.

Table S2 *FOXD3-AS1* transcript levels in 64 NB patients (GSE12460)

Case	*MYCN* amplification	INSS Stage	Tumor type	*FOXD3-AS1* transcript levels
1	No	4	NB	3.9
2	Yes	1	NB	3.04
3	No	3	NB	1.81
4	No	1	GN	7.29
5	Yes	4	NB	4.51
6	Yes	4	NB	3.41
7	No	unknown	NB	5.07
8	Yes	unknown	NB	1
9	No	4	NB	1.07
10	No	4	NB	1.93
11	Yes	3	NB	5.06
12	No	1	NB	1.54
13	No	2b	NB	1.14
14	No	4	GNB	0.26
15	Yes	3	NB	4.13
16	No	unknown	NB	0.93
17	No	4	NB	0.26
18	Yes	unknown	NB	2.41
19	No	1	GN	7.41
20	No	1	NB	4.72
21	No	3	NB	2.1
22	No	1	GNB	5.26
23	Yes	4	NB	0
24	No	4S	NB	2.17
25	Yes	4	NB	4.84
26	No	3	NB	4.39
27	No	3	NB	4.05
28	No	2a	GNB	7.34
29	No	unknown	GNB	6.2
30	Yes	4	NB	1
31	No	2a	GNB	7.4
32	No	2b	NB	0.68
33	No	4S	NB	4.72
34	No	2	NB	3.35
35	No	4	NB	3.29
36	Yes	2b	NB	5.4
37	Yes	4	NB	2.74
38	No	1	NB	2.1
39	No	2	GN	6.65
40	No	unknown	NB	7.01
41	No	4S	NB	0.49
42	No	4S	NB	1.26
43	No	2b	NB	4.1
44	No	4S	NB	2.79
45	No	1	NB	5.35
46	No	4S	NB	3.49
47	No	1	NB	4.56
48	No	4S	NB	0
49	Yes	4	NB	1.72
50	No	2a	NB	1.89
51	No	2b	NB	4.45
52	No	4S	NB	4.78
53	Yes	unknown	NB	0.85
54	No	4	NB	4.1
55	No	1 or 2	NB	3.9
56	No	4	NB	3.05
57	No	1	NB	1.2
58	No	2b	NB	5.38
59	No	4	NB	4.26
60	No	2	GNB	5.64
61	No	2	unknown	5.78
62	No	2	unknown	1.2
63	No	4	NB	0.26
64	No	2	NB	0

Table S3 ***FOXD3-AS1*** **transcript levels in 88 NB patients (GSE16476)**

Case	Age (>18 months)	Gender	*MYCN* amplification	INSS Stage	Progression	Survival time (months)	Death	*FOXD3-AS1* transcript levels
1	No	F	No	2	No	262.5	No	1.14
2	No	M	No	2	No	163.8	No	1.68
3	No	F	No	4S	Yes	248.5	No	0.93
4	No	M	No	2	No	230.1	No	4.04
5	No	F	No	2	Yes	238.2	No	0.77
6	No	M	No	4	No	238.9	No	1.43
7	Yes	F	No	4	Yes	16.2	Yes	4.81
8	Yes	F	Yes	4	Yes	42.5	Yes	0.77
9	Yes	F	No	4	Yes	19.2	Yes	0
10	Yes	F	No	4	Yes	20.3	Yes	3.94
11	Yes	M	Yes	4	Yes	11.3	Yes	0
12	Yes	M	Yes	4	Yes	9.86	Yes	0.68
13	Yes	F	Yes	4	Yes	13.1	Yes	0.93
14	Yes	F	No	4	Yes	46.9	Yes	2.49
15	Yes	M	Yes	4	Yes	6.5	Yes	3.71
16	Yes	M	Yes	4	No	97.2	No	1.43
17	No	M	No	3	No	3.6	Yes	3.43
18	No	M	No	3	No	133.7	No	7.11
19	No	M	Yes	4	Yes	28.8	Yes	0.77
20	No	M	No	4	No	229.1	No	2.29
21	No	M	No	2	No	181.9	No	2.43
22	No	F	No	4S	No	200.4	No	1.63
23	Yes	M	No	4	Yes	5.5	Yes	2.14
24	No	M	No	4S	No	191.9	No	0
25	No	M	No	3	No	170.6	No	4.43
26	No	F	No	4S	Yes	156.4	No	2.58
27	No	F	No	2	No	138.4	No	2.14
28	No	M	No	3	No	136.3	No	1.32
29	No	M	No	4S	No	229.3	No	3.6
30	No	M	No	3	No	243.8	No	4.76
31	Yes	F	No	1	No	208.8	No	4.57
32	Yes	F	Yes	4	Yes	2.1	Yes	3.04
33	Yes	M	No	4	No	9.8	Yes	1.68
34	No	M	No	2	Yes	223.4	No	2.87
35	No	M	No	4	No	229.8	No	2.14
36	No	F	No	1	No	113.8	No	5.93
37	Yes	M	No	4	Yes	9.4	Yes	0.26
38	No	F	No	4S	Yes	82.1	No	1.14
39	No	F	No	2	No	100.7	No	3.77
40	No	M	No	1	No	115.4	No	3.79
41	Yes	M	No	4	Yes	4.2	Yes	0
42	No	M	No	3	No	186.6	No	3.49
43	No	F	No	4S	No	202.3	No	4.19
44	Yes	F	No	3	No	175.8	No	3.19
45	No	M	No	4	Yes	8.5	Yes	2
46	Yes	F	No	4	No	190.1	No	1.54
47	Yes	M	No	4	Yes	17.4	Yes	2.54
48	Yes	M	No	2	Yes	15.2	Yes	2.38
49	No	F	No	4S	No	152.3	No	0.26
50	No	M	No	2	No	118.7	No	3.05
51	No	M	No	1	No	124.9	No	1.49
52	No	F	No	2	No	123.4	No	1.72
53	No	M	No	2	No	146.4	No	5.35
54	Yes	M	No	4	No	129.5	No	1.89
55	No	M	No	3	No	141.5	No	0

56	No	M	No	4S	No	66.4	No	3.35
57	Yes	M	No	3	No	106.4	No	2.87
58	Yes	M	No	4	No	14.7	Yes	2.7
59	No	F	No	4S	No	203.2	No	1.85
60	No	F	No	4	No	128.5	No	0.85
61	Yes	M	Yes	4	Yes	18.4	Yes	3.02
62	No	F	No	4	No	202	No	1.14
63	No	M	No	1	No	146.1	No	0.77
64	No	M	No	3	No	170.8	No	0.14
65	Yes	M	No	4	Yes	7.3	Yes	3.86
66	Yes	M	Yes	4	Yes	39.2	Yes	0.14
67	No	F	No	2	No	123.5	No	3.86
68	No	M	No	1	No	125.7	No	2.17
69	Yes	F	No	4	Yes	9.8	Yes	0.93
70	Yes	M	No	4	Yes	13.2	Yes	0
71	No	F	Yes	4	No	120.8	No	3
72	No	M	No	1	No	102	No	0
73	Yes	M	Yes	4	Yes	8	Yes	0.49
74	Yes	M	No	4	No	77.1	No	3.39
75	Yes	F	No	4	Yes	18	Yes	2.17
76	No	M	No	2	No	69.7	No	2.81
77	Yes	M	No	3	Yes	16.3	Yes	1.32
78	Yes	M	No	1	No	191.7	No	0
79	No	M	No	4S	No	161.9	No	0.26
80	No	F	No	3	No	115	No	3.02
81	Yes	F	Yes	4	Yes	10.8	Yes	1.38
82	Yes	F	No	4	Yes	22.2	Yes	0.26
83	Yes	M	No	2	No	108.7	No	1.93
84	Yes	F	Yes	4	Yes	12.8	Yes	1.54
85	Yes	M	Yes	4	Yes	25.2	Yes	0
86	Yes	M	No	4	No	89.4	No	3.55
87	Yes	F	Yes	3	Yes	5.9	Yes	0
88	No	F	No	4S	No	219.2	No	0.49

F, female; M, male.

Table S4 ***FOXD3-AS1*** **transcript levels in 42 NB patients**

Case	Age (months)	Gender	*MYCN* amplification	INSS Stage	Histology	Survival time (months)	Death	*FOXD3-AS1* transcript levels *
1	6.2	F	No	4	PD	18.1	No	0.435
2	5.3	F	No	4S	PD	18.2	Yes	0.421
3	17.1	M	No	2	PD	18.0	Yes	0.421
4	10.2	M	No	4S	PD	17.3	Yes	0.412
5	16.3	F	No	4S	PD	17.1	Yes	0.381
6	8.1	F	No	4S	PD	16.0	Yes	0.381
7	9.2	M	No	2	PD	16.2	Yes	0.372
8	33.5	F	No	4S	PD	16.3	Yes	0.365
9	22.4	M	No	4	PD	15.1	Yes	0.365
10	58.2	M	Yes	4S	PD	15.3	Yes	0.265
11	8.1	M	Yes	3	PD	9.2	Yes	0.212
12	9	M	No	2	WD	48.1	No	0.842
13	18.3	M	No	2	WD	36.3	No	0.823
14	35.1	F	No	1	WD	41.4	No	0.808
15	23.3	M	No	2	WD	38.1	No	0.786
16	18.2	F	No	1	WD	21.2	No	0.765
17	10.4	M	No	3	WD	19.0	Yes	0.742
18	16.5	M	No	3	WD	13.2	Yes	0.712
19	8.2	M	No	2	WD	32.1	No	0.648
20	7.3	M	No	2	WD	24.1	No	0.632
21	11.3	F	Yes	4S	PD	15.3	Yes	0.121
22	7.4	M	No	4S	PD	12.2	Yes	0.436
23	5.2	M	Yes	4	PD	11.3	Yes	0.118
24	6.1	M	No	4	PD	11.4	Yes	0.352
25	9.3	M	No	3	PD	10.1	Yes	0.343
26	8.2	F	No	2	WD	35.3	No	0.616
27	7.2	M	Yes	1	WD	22.2	Yes	0.456
28	7.1	M	No	1	WD	19.1	No	0.565
29	10.2	M	Yes	3	WD	35.3	No	0.456
30	6.1	M	No	2	WD	18.1	No	0.564
31	19.4	F	Yes	3	PD	12.2	Yes	0.113
32	19.3	F	No	3	WD	10.1	Yes	0.534
33	28.2	M	No	3	PD	23.2	No	0.322
34	30.1	M	No	3	PD	13.3	Yes	0.302
35	36.3	M	No	3	PD	17.2	Yes	0.298
36	45.1	M	Yes	4	PD	11.2	Yes	0.101
37	18.5	F	No	2	WD	34.4	No	0.529
38	20.3	F	No	3	WD	33.1	No	0.495
39	26.5	M	No	3	WD	30.1	No	0.491
40	32.2	M	No	3	WD	33.0	No	0.486
41	41.6	M	No	3	PD	15.5	Yes	0.285
42	43.2	M	Yes	4	WD	34.2	No	0.354

F, female; M, male; PD, poor differentiation; WD, well differentiation. * normalized to transcript levels in normal dorsal ganglia.

Table S5 Mass spectrometry analysis of protein pulled down by biotin-labeled FOXD3-AS1

SH-SY5Y			SK-N-SH		
FOXD3-AS1 AS	**FOXD3-AS1**	**Differential protein**	**FOXD3-AS1 AS**	**FOXD3-AS1**	**Differential protein**
ACTN1	ACTN1	ACTR3	ADH5	ADH5	ATAD1
ACTN4	ACTN4	ANXA3	ADRM1	ADRM1	BTF3
ANXA1	ACTR3	BAG3	ADSL	ADSL	FABP5
ANXA2	ANXA1	CDK13	AHCY	AHCY	FAH
ANXA5	ANXA2	CDK15	AK2	AK2	FUBP3
BAG6	ANXA3	CHD4	AK3	AK3	HIST1H2BM
CDK1	ANXA5	CHD5	ALDOA	ALDOA	HNRNPA0
CDK12	BAG3	COPB2	ALDOC	ALDOC	HNRNPLL
CDK14	BAG6	DDX21	ATP2A1	ATAD1	KIF5B
CDK16	CDK1	DDX27	BUB3	ATP2A1	MAPK3
COPB1	CDK12	ENO1	CAP1	BTF3	PARP1
EEF1A1	CDK13	H2AFV	CAPN2	BUB3	PFDN6
EEF1A1P5	CDK14	H2AFX	CCT4	CAP1	PGAM5
EEF1B2	CDK15	HNRNPDL	CCT5	CAPN2	STMN2
ENO2	CDK16	INTS3	CDK15	CCT4	TUBA1C
H2AFJ	CHD4	INTS4	CDK16	CCT5	
H2AFZ	CHD5	KRT17	CDK17	CDK15	
H2BFS	COPB1	PARP1	DDX3Y	CDK16	
HIST1H2AA	COPB2	TUBA3C	DDX5	CDK17	
HIST1H2AB	DDX21		ELAVL1	DDX3Y	
HIST1H2AC	DDX27		FAM49B	DDX5	
HIST1H2AD	EEF1A1		HIST1H2BK	ELAVL1	
IDH1	EEF1A1P5		HIST1H2BN	FABP5	
IDH2	EEF1B2		HNRNPCL3	FAH	
KRT16	ENO1		HNRNPCL4	FAM49B	
KRT2	ENO2		KRT5	FUBP3	
PCNA	H2AFJ		KRT6A	HIST1H2BK	
S100A11	H2AFV		S100A11	HIST1H2BM	
TUBA1A	H2AFX		STIP1	HIST1H2BN	
TUBA1C	H2AFZ			HNRNPA0	
TUBA3E	H2BFS			HNRNPCL3	
YBX1	HIST1H2AA			HNRNPCL4	
	HIST1H2AB			HNRNPLL	
	HIST1H2AC			KIF5B	
	HIST1H2AD			KRT5	
	HNRNPDL			KRT6A	
	IDH1			MAPK3	
	IDH2			PARP1	
	INTS3			PFDN6	
	INTS4			PGAM5	
	KRT16			S100A11	
	KRT17			STIP1	
	KRT2			STMN2	
	PARP1			TUBA1C	
	PCNA				
	S100A11				
	TUBA1A				
	TUBA1C				
	TUBA3C				
	TUBA3E				
	YBX1				

Table S6 Mass spectrometry analysis of protein pulled down by PARP1 antibody

SH-SY5Y			BE(2)-C		
Mock	**FOXD3-AS1**	**Differential protein**	**Mock**	**FOXD3-AS1**	**Differential protein**
AKR1B1	AKR1B1	BANP	ACTA1	ACTA1	BMI1
BANP	DAD1	CTCF	ACTA2	ACTA2	CDK8
CTCF	DARS	DDX5	APTX	APTX	CTCF
DAD1	DDB1	DHFR	BANF1	BANF1	HIST1H1C
DARS	DDOST	EEF1A1	BMI1	DDX17	HIST1H1D
DDB1	DDX17	EEF1B2	CDK8	DDX39B	HIST1H1E
DDOST	EEF1A1P5	GDI1	CTCF	DDX3X	KRT16
DDX17	EWSR1	GDI2	DDX17	DDX3Y	KRT2
DDX5	FLNA	HIST2H2AC	DDX39B	E2F1	TUBA4A
DHFR	FLNB	HIST2H2BF	DDX3X	EEF1A1	TUBB
EEF1A1	H2AFJ	HIST2H3A	DDX3Y	EEF1A1P5	TUBB4A
EEF1A1P5	H2AFV	KRT1	E2F1	EEF1B2	TUBB4B
EEF1B2	H2AFX	KRT10	EEF1A1	H2AFJ	
EWSR1	HIST1H2AA	KRT14	EEF1A1P5	H2AFV	
FLNA	HIST1H2AB	NDUFV1	EEF1B2	H2AFX	
FLNB	HIST1H2AC	NEDD4	H2AFJ	HSPA4	
GDI1	HNRNPK	PCNA	H2AFV	HSPA5	
GDI2	KRT16	TUBB4B	H2AFX	HSPA8	
H2AFJ	KRT17	TUBB6	HIST1H1C	IDH1	
H2AFV	MCM6		HIST1H1D	IDH2	
H2AFX	MCM7		HIST1H1E	IDH3A	
HIST1H2AA	MDH1		HSPA4	KRT17	
HIST1H2AB	NEDD8		HSPA5	NMT1	
HIST1H2AC	PAK1		HSPA8	NONO	
HIST2H2AC	PAK2		IDH1	SP1	
HIST2H2BF	PARK7		IDH2		
HIST2H3A	PHB		IDH3A		
HNRNPK	SLC25A12		KRT16		
KRT1	SLC25A3		KRT17		
KRT10	TUBB4A		KRT2		
KRT14			NMT1		
KRT16			NONO		
KRT17			SP1		
MCM6			TUBA4A		
MCM7			TUBB		
MDH1			TUBB4A		
NDUFV1			TUBB4B		
NEDD4					
NEDD8					
PAK1					
PAK2					
PARK7					
PCNA					
PHB					
SLC25A12					
SLC25A3					
TUBB4A					
TUBB4B					
TUBB6					

Table S7 Primer sets used for RACE, qPCR, RIP, probe, and ChIP

Primer set	Primers	Sequence	Product size (bp)	Application
FOXD3-AS1	GSP1	5'-GACAGACAGGGATTGGGTT-3'		3'-RACE
	GSP2	5'-GAATAGTTGCCGAGAGAAA-3'		5'-RACE
	NGSP1	5'-CAACTAGGCGGCCTTGCAC-3'		3'-RACE
	NGSP2	5'-AGAAGCCATAACTGGCTAC-3'		5'-RACE
FOXD3-AS1	Forward	5'-GAATAGTTGCCGAGAGAAA-3'	322	qPCR
	Reverse	5'-GACAGACAGGGATTGGGTT-3'		
FOXD3-AS1	Forward	5'-GGAGGAGGCGAGGATGTGTG-3'	310	RIP, probe
	Reverse	5'-TGGTGTGTCTAGGCCAAGGA-3'		
FOXD3	Forward	5'-GACGACGGGCTGGAAGAGAA-3'	161	qPCR
	Reverse	5'-GCCTCCTTGGGCAATGTCA-3'		
IFIT2	Forward	5'- ATCTCTTCCGTGTCTGTTCC-3'	228	qPCR
	Reverse	5'-TCTCCCTTGATTTCTGGTTT-3'		
IL6ST	Forward	5'-CCAAAGGACCTACTGTTCG-3'	235	qPCR
	Reverse	5'-TCATCTGTGTATGCTGCCA-3'		
KLF6	Forward	5'-CTCCACGCCTCCATCTTCT-3'	135	qPCR
	Reverse	5'-TCGCCATTTCCCTTGTCAC-3'		
SAMD9	Forward	5'-GGCAGAGTGGAGATGTGTGGA-3'	137	qPCR
	Reverse	5'-AAAAGCGGGAGTGATGGGTAT-3'		
NEFL	Forward	5'-CTGCCTACGGCGGTTTAC-3'	156	qPCR
	Reverse	5'-CTTCAGAGGGGGGCTCAT-3'		
NPY	Forward	5'-GCTAGGTAACAAGCGACT-3'	186	qPCR
	Reverse	5'-CTCTGCCTGGTGATGAGG-3'		
SCG10	Forward	5'-GGCCAGGCTTTTGAGCTGATCTT-3'	181	qPCR
	Reverse	5'-CCCTCTTCTCTGCCAATTGTTTC-3'		
GAPDH	Forward	5'-AGAAGGCTGGGGCTCATTTG-3'	258	qPCR
	Reverse	5'-AGGGGCCATCCACAGTCTTC-3'		
U1	Forward	5'-ACTTACCTGGCAGGGGAGATACC-3'	137	qPCR
	Reverse	5'-CCACTACCACAAATTATGCAGTCG-3'		
FOXD3 (-859/-610)	Forward	5'-AGAAGGGCGGAAGGGAGAGG-3'	250	ChIP
	Reverse	5'-TCAACAAAGGGACGAGAGAC-3'		
IFIT2 (-689/-524)	Forward	5'-AACTACTTTTGGAATGCTTGCC-3'	166	ChIP
	Reverse	5'-CCCATCTTTGCTCTGCCTTATA-3'		
IL6ST (-334/-98)	Forward	5'-CTCCAGTTCATGACCCCGTT-3'	237	ChIP
	Reverse	5'-GCCCCTGAGAGACCCTTTGC-3'		
KLF6 (-535/-319)	Forward	5'-GAAGGGGACGGGGGGGAA-3'	217	ChIP
	Reverse	5'-CGGCCGGAGCTAAGGGAG-3'		
SAMD9 (-274/-51)	Forward	5'-TGGTTGCAAGACAAAGGAC-3'	224	ChIP
	Reverse	5'-GTGGAGGTAGCAGGGGAGT-3'		
FOXD3-AS1 Set 1	Forward	5'-CCCCTCACTTAGCCCGCCTT-3'	232	ChIP
(-293/-62)	Reverse	5'-CCGCCTCCCGCTGGATCTTT-3'		
FOXD3-AS1 Set 2	Forward	5'-TCCTTCTCTTCCAGCCCGTC-3'	180	ChIP
(-716/-537)	Reverse	5'-AGCCCCCGAACACCCTCATC-3'		

GSP, gene specific primer; NGSP, nested gene specific primer; FOXD3-AS1, forkhead box D3 antisense RNA 1; IFIT2, interferon induced protein with tetratricopeptide repeats 2; IL6ST, interleukin 6 signal transducer; KLF6, Kruppel like factor 6; SAMD9, sterile alpha motif domain containing 9; NEFL, neurofilament light chain; NPY, neuropeptid Y; SCG10, superior cervical ganglia-10; GAPDH, glyceraldehyde 3-phosphate dehydrogenase; RACE, rapid amplification of cDNA ends; RIP, RNA immunoprecipitation; ChIP, chromatin immunoprecipitation.

Table S8 Oligonucleotide sets used for constructs

Oligo Set	Sequences
pcDNA3.1-FOXD3-AS1 (Exon 1+2+3+4)	5'-CGGGGTACCAGGGAATTGTCAACAAAGGGACGA-3' (sense); 5'-GCCGCTCGAGGATTTTTAAATTTTTATTTTTATTTTATTGAATTATTTTTGGTGTGTCT A-3' (antisense)
pcDNA3.1-FOXD3-AS1 (Exon 2+3+4)	5'-CGGGGTACCCTTTAAAGAGTAAGAGCAGCGCAC-3' (sense); 5'-GCCGCTCGAGGATTTTTAAATTTTTATTTTTATTTTATTGAATTATTTTTGGTGTGTCT A-3' (antisense)
pcDNA3.1-FOXD3-AS1 (Exon 3+4)	5'-CGGGGTACCGTGTGGACAAATCCTCCAAGATTT-3' (sense); 5'-GCCGCTCGAGGATTTTTAAATTTTTATTTTTATTTTATTGAATTATTTTTGGTGTGTCT A-3' (antisense)
pcDNA3.1-FOXD3-AS1 (Exon 4)	5'-CGGGGTACCGCCGCCTAGTTGGGAGCCGCAAGA-3' (sense); 5'-GCCGCTCGAGGATTTTTAAATTTTTATTTTTATTTTATTGAATTATTTTTGGTGTGTCT A-3' (antisense)
pcDNA3.1-FOXD3-AS1 (antisense)	5'-CGGGGTACCGATTTTTAAATTTTTATTTTTATTTTATTGAATTATTTTTGGTGTGTCTA -3' (sense); 5'-GCCGCTCGAGAGGGAATTGTCAACAAAGGGACGA-3' (antisense)
pCMV-FLAG-PARP1	5'-CGGAAGATCTGATGGCGGAGTCTTCGGATAAGCTCT-3' (sense); 5'-CTAGTCTAGATTACCACAGGGAGGTCTTAAAATTG-3' (antisense)
pCMV-FLAG-PARP1 (ZnF)	5'-CGGAAGATCTGATGGCGGAGTCTTCGGATAAGCTCT-3' (sense); 5'-CTAGTCTAGACGAGGCTGTGGAGGGCGGAGGCGT-3' (antisense)
pCMV-FLAG-PARP1 (BRCT-WGR)	5'-CGGAAGATCTGGCTCCTGCTGCTGTGAACTCCTCTG-3' (sense); 5'-CTAGTCTAGACTTGGTGCCAGGATTTACTGTCAGC-3' (antisense)
pCMV-FLAG-PARP1 (CAT)	5'-CGGAAGATCTGTCCAAGCTCCCCAAGCCAGTTCAGG-3' (sense); 5'-CTAGTCTAGATTACCACAGGGAGGTCTTAAAATTG-3' (antisense)
pCMV-FLAG-PARP1 (△CAT)	5'-CGGAAGATCTGATGGCGGAGTCTTCGGATAAGCTCT-3' (sense); 5'-CTAGTCTAGACTTGGTGCCAGGATTTACTGTCAGC-3' (antisense)
pCMV-FLAG-PARP1 (△ZnF)	5'-CGGAAGATCTGGCTCCTGCTGCTGTGAACTCCTCTG-3' (sense); 5'-CTAGTCTAGATTACCACAGGGAGGTCTTAAAATTG-3' (antisense)
pGEX-6P-1-PARP1	5'-TCCCCCCGGGGATGGCGGAGTCTTCGGATAAGCTCT-3' (sense); 5'-GCCGCTCGAGTTACCACAGGGAGGTCTTAAAATTG-3' (antisense)
pGEX-6P-1-PARP1 (ZnF)	5'-TCCCCCCGGGGATGGCGGAGTCTTCGGATAAGCTCT-3' (sense); 5'-GCCGCTCGAGCGAGGCTGTGGAGGGCGGAGGCGT-3' (antisense)
pGEX-6P-1-PARP1 (BRCT-WGR)	5'-TCCCCCCGGGGGCTCCTGCTGCTGTGAACTCCTCTG-3' (sense); 5'-GCCGCTCGAGCTTGGTGCCAGGATTTACTGTCAGC-3' (antisense)
pGEX-6P-1-PARP1 (CAT)	5'-TCCCCCCGGGGTCCAAGCTCCCCAAGCCAGTTCAGG-3' (sense); 5'-GCCGCTCGAGTTACCACAGGGAGGTCTTAAAATTG-3' (antisense)
pGEX-6P-1-PARP1 (△CAT)	5'-TCCCCCCGGGGATGGCGGAGTCTTCGGATAAGCTCT-3' (sense); 5'-GCCGCTCGAGCTTGGTGCCAGGATTTACTGTCAGC-3' (antisense)
pGEX-6P-1-PARP1 (△ZnF)	5'-TCCCCCCGGGGGCTCCTGCTGCTGTGAACTCCTCTG-3' (sense); 5'-GCCGCTCGAGTTACCACAGGGAGGTCTTAAAATTG-3' (antisense)
pCMV-Myc-CTCF	5'-CGCGGATCCATGGAAGGTGATGCAGTCGAAGCCA-3' (sense); 5'-GCCGCTCGAGTCACCGGTCCATCATGCTGAGGATC-3' (antisense)
pCMV-Myc-CTCF (N-terminal)	5'-CGCGGATCCATGGAAGGTGATGCAGTCGAAGCCA-3' (sense); 5'-GCCGCTCGAGCTCATCAGTGTGGCTTTTCATGTGA-3' (antisense)
pCMV-Myc-CTCF (ZnF)	5'-CGCGGATCCAGACCACACAAGTGCCATCTCTGTG-3' (sense); 5'-GCCGCTCGAGATTATCAGCATGTCTTGCCATGGTA-3' (antisense)
pCMV-Myc-CTCF	5'-CGCGGATCCTGTGCTGGCCCAGATGGCGTAGAGG-3' (sense);

(C-terminal)	5'-GCCGCTCGAGTCACCGGTCCATCATGCTGAGGATC-3' (antisense)
pCMV-Myc-CTCF	5’-GCGTTATACAGCGGCGGGCAAAGATGTAGATGTGTCTGTCTACGATT-3’ (sense-1);
(Mut)	5’-ACATCTTTGCCCGCCGCTGTATAACGCAGTTTGCTCTTTTTGGTTTT-3’ (antisense-1)
	5’-CTACGATTTTGCGGCAGCACAGCAGGCGGGTCTGCTATCAGAGGTTAATGCAGAGA AAG -3’ (sense-2);
	5’-GATAGCAGACCCGCCTGCTGTGCTGCCGCAAAATCGTAGACAGACACATCTACATC TTT’ (antisense-2)
	5’-TCTGCTATCAGAGGTTAATGCAGAGAAAGTGGTTGGTAATATGAAGCCTCCAAAGC-3’ (sense-3);
	5’-CCAACCACTTTCTCTGCATTAACCTCTGATAGCAGACCCGCCTGCTGTGCTGCCGC -3’ (antisense-3)
pBiFC-VN173-PARP1	5'-CGGAAGATCTGATGGCGGAGTCTTCGGATAAGCTCT-3' (sense);
	5'-CTAGTCTAGACCACAGGGAGGTCTTAAAATTGAAT-3' (antisense)
pBiFC-VC155-CTCF	5'-CCGGAATTCGGATGGAAGGTGATGCAGTCGAAGCCA-3' (sense);
	5'-CCGCTCGAGCCCGGTCCATCATGCTGAGGATCATC-3' (antisense)
pGL3-FOXD3	5'-GGAAGATCTGCCTAAATGAGGGAGGAAAG-3' (sense);
(-1870/+130)	5'-CCCAAGCTTAACCTGCGTCGCTGTCCTTCTCTTCC-3' (antisense)
pGL3-FOXD3	5'-CGTGCCCCATATATGCTGGCGCACAGTGCGGAGCGGAGTTG-3' (sense);
(CTCF Mut)	5'-CGCCAGCATATATGGGGCACGGAGGGCGCTGCGGCCCGCCC-3' (antisense)
pGL3-FOXD3-AS1	5'-CGGGGTACCGGGTCATCCCTCCTCGGGGTTGGT-3' (sense);
(-607/+35)	5'-GCCGCTCGAGTTGCGCGTCTCTCGTCCCTTTGTT-3' (antisense)
pGL3-FOXD3-AS1	5'-GCCTTCCTCGATTGCTGGCCCTGGCGTGGGGCGCAGGAGCGGTCC-3' (sense);
(RXRα Mut)	5'-GCCAGGGCCAGCAATCGAGGAAGGCGGGCTAAGTGAGGGGGCGCG-3' (antisense)

FOXD3-AS1, forkhead box D3 antisense RNA 1; PARP1, poly(ADP-ribose) polymerase 1; CTCF, CCCTC-binding factor; BiFC, bimolecular fluorescence complementation; RXRα, retinoic X receptor alpha.

Table S9 Oligonucleotide sets used for short hairpin RNAs and small interfering RNAs

Oligo Set	Sequences
sh-Scb	5'-AGGGATACAAGCATATACCACTCGAGTGGTATATGCTTGTATCCCTC-3' (sense); 5'-GAGGGATACAAGCATATACCACTCGAGTGGTATATGCTTGTATCCCT-3' (antisense)
sh-FOXD3-AS1 #1	5'-GATCCCGTGTGGACAAATCCTCCAAGACTCGAGTCTTGGAGGATTTGTCCACACTTTT TGGAT-3' (sense); 5'-AGCTATCCAAAAAGTGTGGACAAATCCTCCAAGACTCGAGTCTTGGAGGATTTGTCC ACACGG-3' (antisense)
sh-FOXD3-AS1 #2	5'-GATCCCGAGGAGTTCCGAGAGGAAATACTCGAGTATTTCCTCTCGGAACTCCTCTTTT TGGAT-3' (sense); 5'-AGCTATCCAAAAAGAGGAGTTCCGAGAGGAAATACTCGAGTATTTCCTCTCGGAACTC CTCGG-3' (antisense)
sh-PARP1 #1	5'-GATCCCGTCCTCATCAAGATGATCTTTCTCGAGAAAGATCATCTTGATGAGGACTTTT TGGAT-3' (sense); 5'-AGCTATCCAAAAAGTCCTCATCAAGATGATCTTTCTCGAGAAAGATCATCTTGATGAG GACGG-3' (antisense)
sh-PARP1 #2	5'-GATCCCGTGGAGTATGAGATCGACCTTCTCGAGAAGGTCGATCTCATACTCCACTTTT TGGAT-3' (sense); 5'-AGCTATCCAAAAAGTGGAGTATGAGATCGACCTTCTCGAGAAGGTCGATCTCATACT CCACGG-3' (antisense)
sh-CTCF #1	5'-CCGGGCCTCTTTCTTGGCAAAGTTTCTCGAGAAACTTTGCCAAGAAAGAGGCTTTTT G-3' (sense); 5'-AATTCAAAAAGCCTCTTTCTTGGCAAAGTTTCTCGAGAAACTTTGCCAAGAAAGAGG C-3' (antisense)
sh-CTCF #2	5'-CCGGGCTGTGTTTCATGAGCGCTATCTCGAGATAGCGCTCATGAAACACAGCTTTTT G-3' (sense); 5'-AATTCAAAAAGCTGTGTTTCATGAGCGCTATCTCGAGATAGCGCTCATGAAACACAG C-3' (antisense)
sh-RXRα #1	5'-CCGGGACCTACGTGGAGGCAAACATCTCGAGATGTTTGCCTCCACGTAGGTCTTTT TG-3' (sense); 5'-GATCCAAAAAGACCTACGTGGAGGCAAACATCTCGAGATGTTTGCCTCCACGTAGG TC -3' (antisense)
sh-RXRα #2	5'-CCGGGGGACATGCAGATGGACAAGACTCGAGTCTTGTCCATCTGCATGTCCCTTTT TG-3' (sense); 5'-GATCCAAAAAGGGACATGCAGATGGACAAGACTCGAGTCTTGTCCATCTGCATGTC CC-3' (antisense)
si-Scb	5'-GAACGAUCGAGUAAACGGAtt-3' (sense); 5'-UCCGUUUACUCGAUCGUUCtt-3' (antisense)
si-PARP1	5'-GUGGAGUAUGAGAUCGACCtt-3' (sense); 5'-GGUCGAUCUCAUACUCCACtt-3' (antisense)
si-CTCF	5'-GCCUCUUUCUUGGCAAAGUtt-3' (sense); 5'-ACUUUGCCAAGAAAGAGGCtt-3' (antisense)

FOXD3-AS1, forkhead box D3 antisense RNA 1; PARP1, poly(ADP-ribose) polymerase 1; CTCF, CCCTC-binding factor; RXRα, retinoic X receptor alpha; sh-Scb, scramble short hairpin RNAs.